

# Spectroscopic Analysis of Two Carbon Rich Post-AGB Stars

B.E. Reddy and David L. Lambert

*Department of Astronomy, University of Texas, Austin, TX  
78712;ereddy,dll@astro.as.utexas.edu*

G. Gonzalez

*Department of Astronomy, University of Washington, Seattle, Washington  
98195;gonzalez@astro.washington.edu*

David Yong

*Department of Astronomy, University of Texas, Austin, TX 78712;tofu@astro.as.utexas.edu*

## ABSTRACT

The chemical compositions of the C-rich pAGB stars IRAS 05113+1347 and IRAS 22272+5424 are determined from high-resolution optical spectra using standard LTE model atmosphere-based techniques. The stars are C, N, and *s*-process enriched suggesting efficient operation of the third-dredge up in the AGB star following a first dredge-up that increased the N abundance. Lithium is present with an abundance requiring Li manufacture. With this pair, abundance analyses are now available for 11 C-rich pAGBs. A common history is indicated and, in particular, the *s*-abundances, especially the relative abundances of light to heavy *s*-process elements, follow recent predictions for the third dredge-up in AGB stars.

*Subject headings:* stars: post-AGB - individual: IRAS 05113+1347 and IRAS 22272+5435  
- stars: abundances

## 1. Introduction

The post-asymptotic giant branch (pAGB) stars, as the immediate successors of AGB stars, can be used to probe nucleosynthesis and mixing processes in AGB stars. The spectra of pAGB stars are simple relative to spectra of AGB and planetary nebulae (PNe). In the case of AGB stars, the presence of numerous molecular lines in their spectra makes it difficult to derive accurate abundances. The central stars of PNe to which pAGBs evolve are so hot

that many elements do not provide lines in optical spectra. General properties of pAGBs are well reviewed by Kwok (1993) and recently by Hrivnak (1997).

In the most advanced AGB stars, the predicted changes of surface composition arise from the (third) dredge-up of material from the He-shell below the H-rich envelope. Principal products added to the envelope and atmosphere are  $^{12}\text{C}$ , and heavy elements synthesised by the *s*-process involving neutron capture on a long timescale. Cool carbon stars, i.e., stars with a carbon-rich ( $\text{C/O} > 1$ ) atmosphere, are Nature’s counterparts to the theoreticians’ advanced AGB stars. Carbon-rich pAGB stars have been identified, and this paper presents abundance analyses of two such stars. Many pAGB stars are *not* C-rich, and many, if not all, of the O-rich pAGB stars are also not enhanced in *s*-process products. Examples include the RV Tauri variables (Giridhar, Lambert, & Gonzalez 2000) at the cool end of the pAGB range, and high galactic latitude B-type supergiants, e.g., LSIV -12°111 (Conlon et al. 1993) towards the hot end of the pAGB range. Evidently, many stars depart the AGB before the third dredge-up has transformed the O-rich giant to a C-rich star.

The number of C-rich pAGB stars for which detailed abundance analyses are available is small: 9 stars in total by Reddy et al. (1997, 1999), and Van Winckel & Reyniers (2000). Their compositions do resemble the predictions for advanced AGB stars, but a large sample of stars is needed to test thoroughly the theoretical predictions. The two pAGB stars - IRAS 05113+1347 and IRAS 22272+5435 - analysed here are classified as C-rich because their near- and far-infrared spectra show emission features at  $3.3\ \mu\text{m}$ ,  $3.4\ \mu\text{m}$ , and  $21\ \mu\text{m}$  attributed to carbon-bearing PAH features (Kwok, Volk, & Hrivnak 1989; Hrivnak, Kwok, & Geballe 1994). Basic data for the two pAGB stars are given in Table 1. In this paper, we present abundance results of these two stars. Our analysis of IRAS 05113+1347 is the first to be published. IRAS 22272+5435 was analyzed previously by Začs et al. (1995). Our results differ significantly from theirs, as we discuss below.

## 2. Observations

Spectra of IRAS 22272+5435 and IRAS 05113+1347 were obtained with the 2.7 m McDonald Observatory and the coudé cross-dispersed echelle spectrograph (Tull et al. 1995) on June 14, 2000 and March 26, 2001, respectively. Spectra have a resolving power of  $R \approx 55,000$  as measured from FWHM of Th emission lines, and S/N ratios of 80 - 400 at  $6500\ \text{Å}$ . The spectra run from  $4000\ \text{Å}$  in the blue to  $8800\ \text{Å}$  in the red with gaps in the orders beyond  $5600\ \text{Å}$ . A high-resolution ( $R \approx 45,000$ ) spectrum for IRAS 05113+1347 was also obtained on December 31, 1999 with 3.5 m Apache Point Observatory telescope and an echelle spectrograph. The spectrum runs from  $4000\ \text{Å}$  in the blue to  $10000\ \text{Å}$  in the red with

overlapping echelle orders.

Spectra have been reduced by standard procedures using the spectral reduction package called IRAF<sup>1</sup>. Telluric lines in the spectrum of IRAS 05113+1347 have been removed by dividing with a spectrum of a rapidly rotating hot star. Selected spectral regions at 6785Å and 7965Å of both pAGB stars are displayed in Figures 1 and 2. Atomic spectra are strikingly similar in both stars (Fig 1). Both stars show strong *s*-process lines. The metallic lines are weak suggesting metal deficiency. IRAS 05113+1347 shows photospheric CN lines (Fig 2). Absence of photospheric CN lines in the spectrum of IRAS 22272+5435 may be due to its higher  $T_{\text{eff}}$ .

### 3. Analysis

#### 3.1. Selection of lines and *gf* values

Selection of clean lines with reliable *gf*-values is very important in reducing uncertainties in the abundances. In selecting lines we made use of the very high resolution spectrum of the cool giant Arcturus (Hinkle et al. 2000), as well as the solar spectrum (Wallace, Hinkle & Livingston 1993). To avoid overcrowding of lines and uncertainties in continuum placement, we examined the green and red parts but not the blue part of the spectra. We limited the analysis to lines of moderate strength, equivalent width ( $W_\lambda$ )  $\leq 200$  mÅ. Our line list comprised about 150 atomic lines belonging to 25 elements.

Choosing accurate *gf*-values is important in the reduction of errors. We concentrated on lines which have well determined *gf*-values experimentally or theoretically. The *gf*-values for most of the Fe I and Fe II lines come from laboratory measurements of either the Oxford or Kiel-Hanover groups; Lambert et al. (1996) discussed the *gf*-value measurements. For other elements, we chose accurate *gf*-values from a variety of sources: Cr (Blackwell et al. 1986a), Si (Garz 1973), Ti I (Blackwell et al. 1986b), V (Whaling et al. 1985), Na, Al (Lambert & Warner 1968), Ca (Smith & Raggett 1981), Y II (Hannaford et al. 1982) and for C, N, and O (Wiese et al. 1996). Li, Sc, and Mn exhibit hyperfine structure (HFS). For Sc and Mn, we adopted HFS data of Kurucz (2000), as discussed by Prochaska & McWilliam (2000). For Li we adopted the HFS and isotopic structure given by Andersen et al. (1984). For the rest of the lines, the *gf*-values come either from R.E. Luck’s compilation (private communication) or Kurucz’s (2000) atomic line list. To check the reliability of the *gf*-

---

<sup>1</sup>IRAF is distributed by the National Optical Astronomical Observatories, which is operated by the Association for Universities for Research in Astronomy, Inc., under contract to the National Science Foundation.

values we derived abundances for the solar spectrum using solar equivalent widths measured either by Meylan et al. (1993) or from our solar spectrum at  $R \approx 60,000$  obtained from the McDonald Observatory 2.7 m telescope. We used the Kurucz (1995) convective solar model with a microturbulence of  $1.15 \text{ km s}^{-1}$ . We accepted all the individual  $gf$ -values which yield abundances within  $\pm 0.2$  dex of mean solar abundances (Grevesse & Sauval 1998) determined using the lines having reliable laboratory  $gf$ -values.

### 3.2. Atmospheric Model Parameters

In this study, we adopted plane parallel, and line blanketed LTE model atmospheres computed by Kurucz (1995) using the ATLAS9 code and extracted from <http://cfaku5.harvard.edu>. Final models were found by interpolation. We assume that the standard helium abundance is appropriate to these pAGB stars. A good discussion of the Kurucz model atmospheres is given by Castelli et al. (1997).

Initial values of model parameters  $T_{\text{eff}}$  and  $\log g$  were estimated from their spectral classification and photometry. Hrivnak (1995) classified IRAS 05113+1347 as G8Ia and IRAS 22272+5435 as G5Ia using low-resolution spectra. The spectral types of G8 and G5 translate into  $T_{\text{eff}}$  of 4260 K and 4460 K, respectively (Böhm-Vitense 1972). We estimate  $\log g \approx 1.0$  from the luminosity class Ia and  $\log g$  tables. The values of  $T_{\text{eff}}$  can also be estimated from intrinsic B-V colors. The interstellar extinction values in the direction of the stars were taken from Hrivnak (1995). The intrinsic B-V colors for supergiants (Böhm-Vitense 1972) yield 5100 K for both stars.

Using these initial estimates, we derived more accurate model parameters:  $T_{\text{eff}}$ ,  $\log g$ , microturbulent velocity ( $\xi_t$ ), and metallicity for the program stars from the high-resolution spectra. The values of  $T_{\text{eff}}$  are derived from the excitation of Fe I lines. We chose 23 Fe I lines with lower excitation potentials ranging from 0.85 eV to 4.6 eV. For a given  $\log g = 1.0$  dex and an assumed  $\xi_t = 5.0 \text{ km s}^{-1}$ , the values of  $T_{\text{eff}}$  are determined from the requirement that the individual Fe I abundances be independent of excitation potentials (Fig 3a, 3b). The values of  $\log g$  are determined from the requirement that neutral and ionized iron lines yield similar abundance for the chosen  $T_{\text{eff}}$ . The values of  $\xi_t$  are derived by forcing a zero slope on the abundances of lines Fe I, Fe II, and Ni I as a function of  $W_\lambda$ . This method was iteratively repeated until we obtained a self-consistent set of parameters. The adopted model parameters are given in Table 2.

### 3.3. Radial Velocities

Radial velocity measurements not only provide information on the systemic velocity, but also yield information on the atmospheric structure: velocity gradients in the atmosphere, dust shells around the stars etc. Radial velocities of various atomic and molecular absorption lines are given in Table 3. With the exception of resonance lines, the atomic lines are of photospheric origin and provide the systemic velocity: the mean heliocentric velocities are  $V_r = 7.6 \pm 1.5 \text{ km s}^{-1}$  for IRAS 05113+1347 and  $-42.4 \pm 1.0 \text{ km s}^{-1}$  for IRAS 22272+5435. The velocity of IRAS 22272+5435 is consistent given the probability of a small amplitude variation with the value  $V_r = -39.7 \pm 0.5 \text{ km s}^{-1}$  also measured using optical lines (Začs et al. 1995). Observations of CO millimeter emission lines also provide an estimate of the systemic velocity provided that the emitting gas is uniformly distributed around a star. These estimates match our velocities:  $V_r = 7.2 \text{ km s}^{-1}$  (Hrivnak & Kwok 1999), and  $-41.0 \pm 1.0 \text{ km s}^{-1}$  (Loup et al. 1993) for IRAS 05113+1347 and IRAS 22272+5435, respectively.

Circumstellar  $\text{C}_2$  and CN lines are seen in the spectra (Fig 4). In the case of IRAS 05113+1347, Photospheric CN but not  $\text{C}_2$  lines are also seen but at the systemic velocity,  $V_r$ . For IRAS 05113+1347, Bakker et al. (1997) reported the detection of  $\text{C}_2$  Swan and Phillips, and CN Red system lines from several vibrational bands. Many rotational lines of the  $\text{C}_2$  bands, as expected for a homonuclear molecule, are seen for each band. The circumstellar lines of the CN bands are restricted to low- $J$  lines. Our measurements of  $\text{C}_2$  Swan 0-2 and 0-3 and CN Red system 1-0 lines shows that they are shifted by  $-10.2 \pm 1.0 \text{ km s}^{-1}$  relative to the systemic velocity, a velocity difference identified as the expansion velocity ( $V_{exp}$ ) of that region of the circumstellar shell containing the  $\text{C}_2$  and CN molecules. This expansion velocity is similar to the estimate of  $13.1 \text{ km s}^{-1}$  from the width of the CO millimeter emission lines (Hrivnak & Kwok 1999).

Our detections of optical circumstellar molecular blue-shifted lines for IRAS 22272+5435 are the first for this star which is too warm to show photospheric molecular lines. Swan system lines give an expansion velocity of  $6.3 \pm 0.3 \text{ km s}^{-1}$  which compares with 8.0 to  $12 \text{ km s}^{-1}$  from the widths of CO millimeter lines (Loup et al. 1993).

#### 3.3.1. Profiles of Alkali Resonance Lines

An exciting observation is the apparent presence of the Li I 6707 Å resonance doublet weakly in absorption in both spectra. But excitement is tempered by the additional observation that the line is displaced redward by about 0.2 Å from the wavelength expected of a photospheric line. Understanding this shift and the line profile is a prerequisite to

determining the stellar lithium abundance.

A clue to the correct interpretation of the Li I line is, in the case of IRAS 05113+1347 provided by inspection of the resonance line profiles of the more abundant alkali atoms Na and K. Figure 5a shows the profiles of the Na I D<sub>1</sub>, the K I 7699Å, and the Li I doublet as observed on 1999 December 31. Emission in the core of the Na I D lines exceeds the local continuum. This emission, which is from the star and not the nightsky, divides the absorption profile into two components which we label A and B. Similar emission may be imagined in the K I line but it is evidently weaker with the line profile more strongly suggesting the presence of the two absorption components. The peak Na I emission is at a velocity of 7 km s<sup>-1</sup>, which is the photospheric/systemic velocity (Table 3). This suggests that emission may arise from a large shell, presumably a part of the expanding circumstellar envelope responsible for the CO millimeter emission. The spectrum from March 26, 2001 does not show Na D emission but the components A and B remain. Profiles of the Li I and K I resonance lines are almost unchanged between the two observations. Emission in the Na D lines, if present in IRAS 22272+5435, is very weak. The absorption for this star consists of at least four components: A and B with the same presumed origins as the A and B components in IRAS 05113+1347, and two additional components assigned an interstellar origin and labelled IS in Figure 5b.

For both stars, absorption component A is redshifted relative to the systemic velocity by about 10 km s<sup>-1</sup>. Similar velocity shifts were found for the two pAGB stars studied previously (Reddy et al. 1999). That the component is similar for four stars suggests that it has a common origin, and is not, for example, simply an intruding interstellar line. Two possibilities may be considered: the component is primarily of photospheric origin but redshifted because the line is preferentially formed in cool downdrafts; the line is formed in infalling circumstellar gas. Present evidence suggests the latter is more probable because it appears that only resonance lines of low ionization potential atoms are affected. If the former explanation were valid, one would expect to see a velocity shift between low excitation lines of Na I, and Ca I (for example) and high excitation lines of C I and O I but Table 3 shows no differences. Of course, the presence of infalling (component A) with outflowing (component B) implies a complicated circumstellar shell but such a juxtaposition is not unknown for giant stars.

If component A is taken to be the photospheric line shifted by convective downflow, central emission is seen in all observations of the Na D and K I profiles. The predicted photospheric K I profile (Fig. 5) is based on the inferred normal abundances for [Fe/H]  $\simeq$  -0.8, and the Kurucz model. The true profiles in the actual convective photospheres are surely somewhat different. The emission with component B constitutes a P Cygni profile

provided by circumstellar alkali atoms. Lithium may be similarly affected.

### 3.4. Abundances

Elemental abundances were determined using the code MOOG (Snedden 1973) in combination with the adopted model atmosphere. Most of the selected lines are unblended and computing abundances from equivalent width measurements works well. For a few elements which suffer from blends and/or hyperfine structure, abundances were determined using spectrum synthesis.

A summary of abundances for IRAS 05113+1347 and IRAS 22272+5435 is given in Table 4 where  $n$  is the number of lines, and  $\sigma$  is the standard deviation representing scatter among lines. The quantity  $\log \epsilon(X) = \log (N_X/N_H)+12$  is the abundance of an element X relative to a hydrogen abundance of 12 on a logarithmic scale. The ratio  $[X/H] = \log \epsilon(X_\star) - \log \epsilon(X_\odot)$  refers to the stellar abundance relative to the solar photospheric abundances of Grevesse & Sauval (1998). The abundances relative to iron  $[X/Fe] = [X/H] - [Fe/H]$  are computed using our derived stellar iron abundances of  $[Fe/H]$ .

Errors in the abundance analysis come from different sources. Errors in the adopted  $gf$ -values and in the measured  $W_\lambda$  introduce uncertainties. These errors can be represented by the standard deviation,  $\sigma$  (Table 4) that measures the scatter among the individual lines. The true error, i.e., standard deviation of the mean  $\sigma/\sqrt{n}$ , is less for elements represented by many lines. For abundances which are derived by fewer than 3 lines the real error may be large, and we adopted  $\sigma = 0.2$  dex for these sources of error.

The abundances are also model dependent. The four parameters:  $T_{\text{eff}}$ ,  $\log g$ ,  $\xi_t$ , and  $[M/H]$  that are required to select the atmospheric model are somewhat coupled. The uncertainty in the  $T_{\text{eff}}$  can be estimated by examining the relation between the lower excitation potential and abundance. The slope of the fit to the observations is quite sensitive to  $T_{\text{eff}}$ . The error (standard deviation) in the slope  $\sim 0.03$  translates into an uncertainty in the  $T_{\text{eff}}$  of 150 K. Similarly, we estimated uncertainty in  $\xi_t$ . In the case of  $\log g$ , the error is estimated by introducing 0.1 dex difference in abundance between neutral and ionized lines. Thus, the estimated uncertainties in the input model parameters are as follows:  $\delta T_{\text{eff}} = 150$  K,  $\delta \log g = 0.50$  dex,  $\delta \xi_t = 0.50$  km s<sup>-1</sup>, and  $\delta [M/H] = 0.25$  dex. The uncertainties in the abundance ratios as a result of uncertainties in the model parameters are given in the Table 5 for IRAS 05113+1345. The values in the Table 5 show that the abundance ratios are less affected by uncertainties in the  $[M/H]$  and  $\xi_t$ . The uncertainty in the gravity of 0.5 dex changes the ratios up to 0.15 dex. The abundance ratios determined from the lines

of high excitation are found to be sensitive to changes in  $T_{\text{eff}}$  (Table 5). For each element the quadratic sum of the uncertainties in the four model parameters is given as  $\sigma_m$ .

Our results for IRAS 22272+5435 differ quite considerably in several key respects from those published by Zács et al. (1995). The differences are not related to slight differences in the adopted fundamental parameters. There is a small difference in the derived iron abundances: we obtain  $[\text{Fe}/\text{H}] = -0.8$  but Zács et al. got  $[\text{Fe}/\text{H}] = -0.5$ . Large differences are found for many other elements. For example, they reported several cases of extraordinary enhancements relative to iron: e.g., ratios for elements around iron include  $[\text{Cr}/\text{Fe}] = +2.0$ ,  $[\text{Ni}/\text{Fe}] = +1.5$ , and  $[\text{Zn}/\text{Fe}] = +2.2$ . In all cases, our ratios are close to the expected values for a moderately metal-poor star, that is  $[\text{Cr}/\text{Fe}] = [\text{Ni}/\text{Fe}] = [\text{Zn}/\text{Fe}] \simeq 0.0$ . Although our analyses agree that the *s*-process elements are severely overabundant, abundances in the two analyses differ by up to 1.0 dex. These differences may perhaps be traceable to the lower resolution of the spectra used by Zács et al., and their tendency to include strong lines in the abundance analysis. Scrutiny of their list of measured lines showed several cases where we identified much weaker lines with the transition that they used.

#### 3.4.1. Carbon, Nitrogen, and Oxygen

The abundance of carbon is determined using three different indicators: permitted C I lines, the forbidden C I line at 8727.1 Å (this line is not measured in the spectrum of IRAS 22272+5435), and lines of the CN red system at 8035 Å. The forbidden C I line is a superior C abundance indicator as it is unaffected by NLTE (Gustafsson et al. 1999). However, this line is blended with Fe I and CN lines. Fortunately, the Fe I and CN contributions to the blend at this metallicity are small. All known blends are taken into account in the spectrum synthesis. For IRAS 05113+1347, the carbon abundance from this forbidden line is 0.2 dex less than that derived using the permitted C I lines, but the error estimate  $\delta T_{\text{eff}} = 150$  K causes a difference of 0.19 dex in abundances derived from permitted and forbidden C I lines. Non-LTE effects may also be a factor. The CN Red system lines yield a higher abundance by 0.3 dex than the forbidden line. This may be due to the uncertainty in the abundance of N which is an input in the synthesis of CN lines and is based on two weak N I lines in the red. Given the uncertainties in the model parameters the derived C and N abundances from different abundance indicators are in good agreement.

The abundance of oxygen is determined using both forbidden and permitted lines. The oxygen abundance ( $\log \epsilon([\text{O I}])=8.37$ ) determined from [O I] lines at 6300.3 Å and 6363.8 Å for IRAS 05113+1347 is found to be in good agreement with the abundance derived from the permitted O I line at 9265.9 Å. For IRAS 22272+5435, the oxygen abundance comes from



the [O I] line at 6300.3 Å. Final results of C, N, and O abundances are given in Table 6. Abundances of C and O are the simple mean of abundances derived using different indicators. Total sum of C, N, and O abundances ( $\Sigma CNO$ ) relative to Fe and ratios C/O and N/O are also given in Table 6.

### 3.4.2. *s*-process elements

A majority of the *s*-process lines used here come from Kurucz’s (2000) line list. Many of these lines do not exist in the solar spectrum. Given the large number of lines in the Kurucz list it is difficult to know that the *s*-process line is the dominant contributor. To make sure, we computed equivalent widths for all the nearby lines. Molecular CN and C<sub>2</sub> contributions to the lines were also taken into account. This procedure allowed us to identify quite a number of reasonably clean *s*-process lines. The *s*-process lines, their atomic data, and abundances are given in the Table 8.

### 3.4.3. *Spectrum Synthesis: Li Abundance*

Extraction of the Li abundance is important because lithium plays an important role in understanding the evolutionary state of pAGB stars. Here, the abundance analysis is complicated by the fact that the dominant absorption attributable to the Li I 6707 Å line is at the velocity of the infalling material labelled as component A. Component B, definitively circumstellar, may also contribute absorption to confuse further a contribution from a Li I photospheric line. Finally, emission may fill-in the photospheric Li I absorption in the case of IRAS 05113+1347. To within the errors of measurement, identical velocity shifts of a line likely to be the photospheric Li I line are found for this pair of pAGBs as well as and the pAGBs IRAS 02229+6208 and IRAS 07430+1115 (Reddy et al. 1999).

Our syntheses of the Li region used atomic lines listed by Kurucz (2000), and CN Red system lines (Cunha, Smith, & Lambert 1995). The Arcturus spectrum was synthesized and, as a result, minor modifications were made to the adopted *gf*-values. We also included the *s*-process ionized line required by Lambert, Smith, & Heath (1993) to fit spectra of Ba II giants. Selected syntheses are shown in Figure 6 where it is obvious that the observed spectrum cannot be matched satisfactorily. These syntheses leave unmatched the absorption to the red that is attributed to a Li I line from the circumstellar shell (component A). The presence of two Li I components is not at all unprecedented having been reported for a Li-rich (O-rich) giant in the globular cluster NGC 362 (Smith, Shetrone, & Keane 1999), and for

the Li-rich semiregular variable, also O-rich, W LMi (Giridhar, Lambert, & Gonzalez 2000). Alternative interpretations seem implausible. If photospheric lithium is assumed to be rich in  ${}^6\text{Li}$ , a fair fit to the spectrum is obtained, as noted previously by Reddy et al. (1999); the  ${}^7\text{Li}$  -  ${}^6\text{Li}$  wavelength shift is about  $7 \text{ km s}^{-1}$  or only slightly less than the redshift of component A, but the presence of  ${}^6\text{Li}$  is considered most improbable. A V I line at  $6708.07\text{\AA}$  might be deemed responsible for component A but the  $gf$ -value needed to fit the line in Arcturus must be increased by nearly 3 dex to match component A in the pAGBs. Finally, it is unlikely that the component is an unrecognized  $s$ -process line; no such line was required by Lambert et al. (1993) in their syntheses of spectra of Ba II giants including stars for which the Ce II lines are of comparable strength to the lines in the pAGB stars. (Technetium appears not to have a line at  $6708.0\text{\AA}$ .)

If component A is assigned to circumstellar lithium atoms and circumstellar emission is neglected, a fair assumption given that the spectrum of IRAS 05113+1347 at  $6707\text{\AA}$  is not significantly different when the Na D emission was very prominent, the syntheses of the photospheric component give  $\log \epsilon(\text{Li}) \simeq 1.8$  for IRAS 05113+1347, and  $\simeq 2.1$  for IRAS 22272+5435.

#### 3.4.4. *Spectrum Synthesis: ${}^{12}\text{C}/{}^{13}\text{C}$ ratio*

To derive the carbon isotopic ratio, we selected lines of the CN Red system in the spectral region  $8000\text{-}8010 \text{ \AA}$ . This is the region where a strong blend of  ${}^{13}\text{C}$  features at  $8000.4 \text{ \AA}$  and clean  ${}^{12}\text{CN}$  lines are located. There are other  ${}^{13}\text{CN}$  features but most of them are buried in stronger  ${}^{12}\text{CN}$  lines. The molecular data: line positions, excitation values, and oscillator strengths are taken from the investigation of de Laverny & Gustafsson (1998; private communication from de Laverny). The list includes all the  ${}^{12}\text{CN}$  lines given by Davis & Philips (1963) and  ${}^{13}\text{CN}$  lines given by Wyller (1966). Additional input data required to produce synthetic spectrum is the dissociation energy that we adopted  $7.75 \text{ eV}$  (see Lambert 1993) for both the molecules. The region  $8000\text{-}8010 \text{ \AA}$  was computed using the adopted line list for the Arcturus model atmospheres and the abundances. The resultant spectrum was compared with the observed high-resolution spectrum of Arcturus to test the accuracy of the molecular and atomic line data. The predicted spectrum matches nicely the observed Arcturus spectrum and this also yields  ${}^{12}\text{C}/{}^{13}\text{C} = 6.0 \pm 1.0$  which is in very good agreement with the isotopic ratio measured for Arcturus (Griffin 1974).

We computed the spectrum for IRAS 05113+1347. (Photospheric CN lines are not seen in the spectrum of IRAS 22272+5435). We fit the  ${}^{12}\text{CN}$  for the derived N abundance by changing the C abundance. For a C abundance of  $8.90 \pm 0.1 \text{ dex}$  the  ${}^{12}\text{CN}$  lines are well

fitted (Fig 7). The  $^{13}\text{CN}$  feature blended with  $^{12}\text{CN}$  at 8002.0 Å, the blends of pure  $^{13}\text{CN}$  line at 8004.5 Å, and at 8006.0 Å are sensitive to the changes in the isotopic ratio  $^{12}\text{C}/^{13}\text{C}$ . The spectrum was predicted for three different carbon isotopic ratios and compared with the observed spectrum of IRAS 05113+1347. The features at 8002.0 Å and 8004.5 Å indicate a lower limit of  $^{12}\text{C}/^{13}\text{C} > 25$ . A slightly smaller value is suggested by the  $^{13}\text{CN}$  feature at 8006.0. We give greater weight to the feature at 8004.5 Å as this is stronger and pure  $^{13}\text{CN}$ . The limit  $^{12}\text{C}/^{13}\text{C} > 25$  is in good agreement with the typical lower limit of  $^{12}\text{C}/^{13}\text{C} \geq 20$  derived for pAGBs, including IRAS 05113+1347, by Bakker et al. (1997) using circumstellar molecular CN red lines.

## 4. Stellar Evolution and Chemical Composition

Inspection of the compositions of the two pAGB stars (Table 4 & 6) leads to four broad conclusions, which we amplify below: (i) their composition is normal except for those elements expected to be affected during evolution prior to the pAGB phase; (ii) lithium is present at an abundance that probably implies lithium production in a post main sequence phase; (iii) adjustments to initial C and N abundances occurred as a result of mixing with H- and He-burnt material; (iv) substantial enrichment with *s*-processed material is traceable to mixing from the He-shell of their AGB progenitor. Collectively, these conclusions suggest the stars have evolved from thermally-pulsing AGB stars. The pair are compared with published results for 9 other C-rich pAGB stars (Table 7), which support the four broad conclusions.

Even in the case of thermally-pulsing AGB stars, many elements are expected to retain their initial abundances (relative to iron). This is the case here: Na, Al, Si, S, Ca, Ti, and the iron-group from V to Ni, and Zn show the ratio  $[X/Fe]$  reported for normal dwarfs and red giants with  $[Fe/H] \simeq -0.8$ . (Possibly,  $[Ca/Fe] \simeq 0.0$  is less than the expected value of 0.2 dex as a result of Galactic chemical evolution.) This demonstration of normal abundances serves to exclude the possibility that the photospheres are affected by processes of dust-gas selective fractionation that are seen to have affected some warmer pAGB stars (Waelkens et al. 1992), and the warmest RV Tauri variables (Giridhar, Lambert, & Gonzalez 1999). In particular, our pair of pAGB stars show normal  $[S/Fe]$  and  $[Zn/Fe]$  ratios which are potent indicators of dust-gas fractionation.

### 4.1. Carbon, Nitrogen, and Oxygen

Carbon, nitrogen, and oxygen abundances are key tracers of the evolutionary and nucleosynthetic history of red giants and their descendants. Low mass red giants are predicted to experience three episodes in which the deep convective envelope brings nuclear-processed material from the interior to the atmosphere. The first episode known as the first dredge-up occurs when the star ascends the red giant branch, after exhaustion of hydrogen in the core of the main sequence star. This brings mildly CN-cycled material to the surface and, therefore, reduces the C abundance and enhances the N abundance with the constraint that the sum of the C and N abundances is preserved (Iben 1964). Oxygen is predicted and observed to be unaffected by the first dredge-up.

Additional changes of surface abundances occur through what is known as the third dredge-up phase known to affect AGB stars. In this phase, material from the He-shell around the C-O electron degenerate core is mixed into the base of the deep convective envelope. The

added material has been exposed to He-burning via the  $3\alpha$ -process and to  $s$ -processing. The principal product of the former is  $^{12}\text{C}$  with an admixture of  $^{16}\text{O}$ . An AGB star is expected to experience the third dredge-up repeatedly until it evolves to the pAGB phase and beyond. (Even then a final episode is possible.) Through the third dredge-up, the O-rich giant may be converted to a C-rich AGB star. In its simplest theoretical implementation, the series of third dredge-up events do not involve exposure of the H-rich envelope to the H-burning CN-cycle, that is the carbon added from the He-shell is not converted to nitrogen. Very luminous AGB stars can experience H-burning at the base of the H-rich envelope in the long intervals between times when the He-shell is ignited. Such stars said to experience hot bottom burning (HBB), convert carbon to nitrogen, reduce the  $^{12}\text{C}/^{13}\text{C}$  ratio, and may be reconverted from a C-rich to an O-rich star.

In order to compare the observed C, N, and O abundances with theoretical expectations, we begin with establishing the initial abundances for these slightly metal-poor stars, and, then, we comment on the changes expected from the first dredge-up which establish the expected surface abundances for the AGB star prior to the onset of the third dredge-up. Observed abundances for our two stars and eight others analysed previously are summarized in Table 6.

Initial abundances for C and O are taken from Gustafsson et al. (1999) who analysed the [C I] 8727 Å line in a sample of main sequence stars, and collated results on the O abundance for a similar and overlapping sample. Fits to the derived abundances gave

$$[C/Fe] = (-0.17 \pm 0.03) \times [Fe/H] + (0.065 \pm 0.008)$$

and

$$[O/Fe] = (-0.36 \pm 0.02) \times [Fe/H] - (0.044 \pm 0.010)$$

Measurements of the nitrogen abundance are less extensive. We adopt  $[N/Fe] = 0$  (Clegg, Lambert, and Tomkin 1981).

The inferred initial abundances are given in Table 6 along with the observed values for the pAGB stars. Relative to initial values, the stars are clearly enriched in carbon and nitrogen, but oxygen has retained about its initial abundance. These are in line with our sketch of the expected changes: the carbon enrichment is attributed to the third dredge-up, and the nitrogen enrichment to the first dredge-up, and, as expected, oxygen is almost unaffected by the dredge-ups.

From Table 6, the mean difference between the O abundance of the pAGB stars and their inferred initial O abundance is 0.2 dex. Given the possibility of systematic errors in comparing abundances derived from main sequence and pAGB stars, this difference is

compatible with the expectation that oxygen is unaffected by evolution from the main sequence to the pAGB stage. It may be noted that a study of post first dredge-up red giants with metallicities similar to those of stars in Table 6 concluded that oxygen was undepleted (Cottrell & Sneden 1986).

There is evidence, primarily from the low observed and higher predicted  $^{12}\text{C}/^{13}\text{C}$  ratios, that predicted changes for carbon and nitrogen brought by the first dredge-up are less severe than observed changes. It is, however, expected that a red giant’s nitrogen abundance will approach the sum of the star’s initial C and N abundances. Considering this, we list in Table 7 this sum alongside the observed N abundances for the pAGB stars. On average, the latter are equal to the sum of the initial C and N abundances: the mean difference is less than 0.1 dex. This is certainly compatible with the idea that the nitrogen abundance of AGB and pAGB stars was unaltered by the third dredge-up and subsequent events.

Cottrell & Sneden’s analyses, however, do not fully support this conclusion. Their carbon abundances show the expected underabundance, for the first dredge-up, especially if the initial abundances are taken from Gustafsson et al. (1999). Low  $^{12}\text{C}/^{13}\text{C}$  ratios reported by the authors clearly show that a first dredge-up has occurred. Oddly, nitrogen was reported to be underabundant:  $[\text{N}/\text{Fe}] = -0.05$  was found in the mean. This is surprising. We suppose that this anomaly is either an artifact of the analysis and/or the assumption that  $[\text{N}/\text{Fe}] = 0$  is incorrect for the initial abundances. If, of course,  $[\text{N}/\text{Fe}] < 0$  initially, our conclusion that the first dredge-up accounts for the observed nitrogen abundances of pAGB stars is invalid.

The first dredge-up reduces the surface  $^{12}\text{C}/^{13}\text{C}$  ratio. Cottrell & Sneden’s measurements give a mean ratio of 16 for their sample of mildly metal-poor giants. Available determinations for the pAGBs including our lower limit for IRAS 05113+1347 give higher values. These are consistent with addition of  $^{12}\text{C}$  to the envelope of a red giant without exposure to the CN-cycle, which would convert some  $^{12}\text{C}$  to  $^{13}\text{C}$  and  $^{14}\text{N}$ . Thus, the  $^{12}\text{C}/^{13}\text{C}$  ratios and the nitrogen abundances support the idea that little of the  $^{12}\text{C}$  from the third dredge-up has been processed by protons.

Carbon in pAGBs is considerably enhanced relative to its initial abundance and certainly to its post first dredge-up abundance. The stars are clearly C-rich, i.e.,  $\text{C}/\text{O} > 1$ . Table 6 shows that  $\text{C}/\text{O} \simeq 3$  for IRAS 05113+1347, and 2 for IRAS 22272+5435. The sensitivities of the abundances to the atmospheric parameters are so similar for the carbon and oxygen lines that the derived C/O ratio cannot be plausibly decreased to less than unity. We assume that fresh carbon was added through the third dredge-up events.

In summary, the C, N, and O abundances are compatible with the view that these C-rich pAGB stars evolved directly from AGB stars that were converted to carbon stars as a result

of the third dredge-up. It remains to examine if the  $s$ -process and lithium abundances may be integrated into this picture.

## 4.2. The $s$ -process

Both stars are severely enhanced in  $s$ -process elements (Table 7) which we identify as a signature that the stars experienced an efficient third dredge-up in their AGB phase. In this respect, our pair of pAGBs are similar to the other analyzed C-rich pAGBs. Models indicate that low mass AGB stars run their  $s$ -processing in the He-shell with the neutron source  $^{13}\text{C}(\alpha, n)^{16}\text{O}$ . To provide sufficient neutrons,  $^{13}\text{C}$  must be generated in the H-He intershell region by a slow mixing of protons into the He-rich layers. Presently, the mass of  $^{13}\text{C}$  in the shell at the onset of  $s$ -processing is not calculable from the first principles but must be specified as a free parameter. This free parameter is a controlling influence on the neutron flux. The higher the neutron flux the greater is the abundance of *heavy* relative to *light*  $s$ -process elements. This is customarily characterized by the ratio [hs/ls] (Luck & Bond 1991) where we take La and Nd as heavy- $s$  (hs) and Y and Zr as light- $s$  (ls) elements. The abundances of these four  $s$ -process elements are represented by several lines and available for all the C-rich pAGBs. Busso et al. (2001) also used the same  $s$ -process elements in their theoretical computations. The results would not be significantly changed if we adopted any other combinations of heavy  $s$ -process elements. The ratios [hs/ls] for 10 pAGBs including the two pAGBs studied here are given in Table 7.

The ratio [hs/ls] varies with metallicity across the pAGB sample. This is clearly shown in Figure 8. For comparison we show the model predictions from Busso et al. (2001) for the case in which the mass of  $^{13}\text{C}$  in the He-shell is assigned a constant and plausible value independent of metallicity. The chosen value designated as ST/1.5 for a model of  $1.5 M_{\odot}$  by Busso et al. offers a good fit to [hs/ls] measurements for  $s$ -process enriched stars over a wide range of metallicity. The model predictions offer a good fit to the observed trend set by the pAGBs. Two pAGB stars (IRAS 07134+1005 and IRAS 02229+6208) deviate from this trend and they can be matched well with ST/3 model predictions. The models also account for the observed enhancements [ls/Fe] and [hs/Fe].

## 4.3. Lithium

At [Fe/H]  $\sim -0.8$ , the maximum lithium abundance seen in main sequence stars is  $\log \epsilon(\text{Li}) \simeq 2.3$  (Chen et al. 2001). At the first dredge-up, the surface lithium abundance is

reduced by a factor of about 50, i.e.,  $\log \epsilon(\text{Li}) \simeq 0.6$  is predicted for red giants. Shetrone, Sneden, & Pilachowski (1993) found lithium abundances from 0.3 to  $< -0.5$  in old disk giants with  $[\text{Fe}/\text{H}]$  similar to that of our pAGBs and a low  $^{12}\text{C}/^{13}\text{C}$  ratio. Hence, the pAGB stars with  $\log \epsilon(\text{Li}) \simeq 2.0$  are very Li-rich relative to their putative progenitors. Therefore, the Li-rich stars have either experienced lithium production, or external replenishment of lithium (e.g., engulfed a planet).

Production is possible by what is known familiarly as the Cameron-Fowler (1971)  $^7\text{Be}$  transport mechanism in which  $^3\text{He}$  by  $\alpha$ -capture is converted to  $^7\text{Be}$  and subsequently to  $^7\text{Li}$  by electron capture. The  $^3\text{He}$  supply is partly primordial  $^3\text{He}$  and partly the product of incomplete running of the  $pp$ -chain in the outer parts of the low mass main sequence star. A high temperature is needed for  $\alpha$ -capture on  $^3\text{He}$  but a low temperature is needed for  $^7\text{Li}$  (and  $^7\text{Be}$ ) to avoid destruction by protons. Thus, lithium production is efficient only in a convective region/envelope with a hot base and cool outer boundary. In intermediate mass (4 to  $7M_{\odot}$ ) AGB stars, predictions and observations show that lithium production is possible. This has been most clearly demonstrated for the most luminous AGB stars in the Magellanic Clouds (Smith & Lambert 1989, 1990; Plez, Smith, & Lambert 1993; Sackmann & Boothroyd 1992). The great majority of these Li-rich stars are O-rich, a not unexpected result because the temperatures required for  $\alpha$ -capture by  $^3\text{He}$  also ignite the CN-cycle which will convert carbon to nitrogen and convert C-rich material to N-rich material with a low  $^{12}\text{C}/^{13}\text{C}$  ( $\sim 3$ ) ratio. Attribution of lithium production to intermediate-mass luminous AGB stars implies that the Li-rich pAGBs evolved from stars with masses of about  $4 M_{\odot}$ , which is unlikely, although perhaps not impossible, for stars as metal-poor as  $[\text{Fe}/\text{H}] \sim -0.8$ .

Examination of the reaction rates shows that the time scales ( $\propto n_i/(dn_i/dt)$ ) for destruction of  $^3\text{He}$  and  $^{12}\text{C}$  are similar over the likely range of temperature. The rate constant for  $^3\text{He}(\alpha, \gamma)^7\text{Be}$  is approximately an order of magnitude greater than for  $^{12}\text{C}(p, \gamma)^{13}\text{N}$  (Angulo et al. 1999) but this difference is offset by the ratio  $\alpha/p \simeq 0.1$ . Then,  $^3\text{He}$  and  $^{12}\text{C}$  are destroyed at about the same rate. Unfortunately, the amount of  $^3\text{He}$  that was destroyed to produce the observed lithium abundance is unknown because the efficiency of the conversion of  $^7\text{Be}$  to  $^7\text{Li}$  is not obtainable from the observations. Certainly, the observed lithium abundance is a small fraction (perhaps, a  $10^6$ th) of the  $^3\text{He}$  reservoir predicted by standard models. Even at low efficiency, a small fractional change in the  $^3\text{He}$  abundance results in the observed lithium abundance with a similarly small fractional change in the  $^{12}\text{C}$  and, hence, the  $^{14}\text{N}$  abundance. Provided that fresh  $^{12}\text{C}$  is added from thermal pulses occurring during and after lithium production, stars can remain C-rich with a high  $^{12}\text{C}/^{13}\text{C}$  ratio yet present a lithium enrichment.

Lithium-rich giants are known at much lower luminosities (cf. Charbonnel & Balachan-



dran 2000). Several proposals exist in which the  $^3\text{He}$  reservoir is tapped to provide the  $^7\text{Li}$ . It is unlikely that these stars are progenitors of the Li-rich pAGBs. The lithium in the giants will most probably be destroyed as the stars evolve to the end up the AGB. Certainly, conversion of these O-rich giants to C-rich AGB (and pAGB) stars will remove the lithium unless it is replenished from the  $^3\text{He}$  reservoir.

Replenishment of lithium is in principle possible when the AGB star engulfs a planet or a brown dwarf. Siess & Livio (1999) discuss accretion by a  $3 M_{\odot}$  AGB star. These calculations suggest that surface lithium is enhanced by a factor of a few, a factor barely sufficient to account for the observed lithium abundances. Although the parameter space of the scenario was not fully explored and other choices of AGB star (e.g., lower mass and lower metallicity) and accreted object may result in a higher lithium abundance, this scheme will have difficulty in accounting for the fact that a lithium enrichment is very common among the C-rich pAGB stars. Five of the 10 stars in Table 7 have been reported to show lithium enrichment. Spectra of the other five stars have been examined for lithium but the  $6707\text{\AA}$  line was apparently absent. Assuming a detection limit of  $5 \text{ m}\text{\AA}$  for the line we obtain the abundance limits shown in Table 7. All are consistent with either lithium enrichment or the low lithium abundance predicted for an AGB star that does not manufacture lithium.

## 5. Conclusions

Our abundance analysis based on high-resolution optical spectra of IRAS 05113+1347 and IRAS 22272+5435 shows that these stars classified as pAGB stars have the surface composition expected of a highly-evolved AGB star: carbon and nitrogen enrichments (relative to their presumed initial abundances) are identified as products of the third and first dredge-ups, respectively, and a strong *s*-process enrichment is also attributable to the third dredge-up. An intriguing lithium enrichment may reflect lithium production from  $^3\text{He}$  in the AGB or pAGB star. The two stars analysed in this paper seem typical of the sample (now, 11 stars in total analysed) of C-rich pAGB stars.

If the transition from AGB to pAGB star was made without drastic alterations of surface composition, the immediate progenitor of a C-rich pAGB was a cool carbon star of the N-type. Bright cool carbon stars analysed by Lambert et al. (1986) and Ohnaka, Tsuji, & Aoki (2000) have C,N, and O abundances quite similar to the pAGBs, and are *s*-process enriched to similar levels too. However, the carbon stars are of approximately solar metallicity (Lambert et al. 1986; Abia et al. 2001) not metal-poor like the pAGBs. Lithium provides a discordant note. The N-type stars are not lithium rich. The lithium-rich carbon stars are the J-type stars rich in  $^{13}\text{C}$  and with no *s*-process enhancement. There are metal-poor carbon stars in

the halo that are as metal-poor as the pAGBs: Kipper et al. (1996) analysed 5 stars with  $[\text{Fe}/\text{H}]$  from  $-0.7$  to  $-1.2$ , all with considerable  $s$ -process enrichments. With one exception, the carbon abundances are similar to those of the pAGBs. But with the same exception, the nitrogen abundances are much less than those of the pAGBs. In two of the stars Li was found to be enhanced ( $\log \epsilon(\text{Li}) \geq 1.7$ ). The noticeable difference is that the  $^{12}\text{C}/^{13}\text{C}$  ratio of the carbon stars are much lower (5 to 10) than the limits set for the pAGBs. In summary, the immediate progenitors of the pAGBs have yet to be identified. This is odd given that the pAGBs evolve rapidly and probably more rapidly than their AGB progenitor. It is quite possible that the progenitor is shrouded by dust.

We acknowledge the support of National Science Foundation (Grant AST-9618414) and the Robert A. Welch Foundation of Houston, Texas. We thank Dr. Pandey and Dr. Allende Prieto for many helpful comments. This research has made use of the Simbad database, operated at CDS, Strasbourg, France, and the NASA ADS service, USA.

## REFERENCES

- Abia, C., Busso, M., Gallino, R., Domínguez, I., Straniero, O., & Isern, J. 2001, *ApJ*, (in Press)
- Andersen, J., Gustafsson, B., & Lambert, D.L. 1984, *A&A*, 136, 75
- Angulo, C., Arnould, M., Rayet, M., (NACRE collaboration), 1999, *Nuclear Physics A*, 656, 1
- Bakker, E.J., van Dishoek, E. F., Waters, L.B.F.M., & Schömaker, T. 1997, *A&A*, 323, 469
- Blackwell, D.E., Booth, A.J., Menon, S.L.R., & Petford, A.D. 1986a, *MNRAS*, 220, 303
- Blackwell, D.E., Booth, A.J., Menon, S.L.R., & Petford, A.D. 1986b, *MNRAS*, 220, 289
- Böhm-Vitense, E. 1972, *A&A*, 17,335
- Busso, M., Gallino, R., Lambert, D.L., Travaglio, C., & Smith, V.V. 2001, *ApJ* (in press)
- Cameron, A.G.W., & Fowler, W.A. 1971, *ApJ*, 164, 111
- Castelli, F., Gratton, R.G., & Kurucz, R.L. 1997, *A&A*, 318, 841
- Charbonnel, C., & Balachandran, S.C. 2000, *A&A*, 359, 563
- Chen, Y.Q., Nissen, P.E., Benoni, T., & Zhao, G. 2001, *A&A*, 371, 943
- Clegg, R.E.S., Tomkin, J., & Lambert, D.L. 1981, *ApJ*, 250, 262
- Conlon, E.S., Dufton, P.L., McCausland, R.J.H., & Keenan, F.P. 1993, *ApJ*, 408, 593
- Cottrell, P.L., & Sneden, C. 1986, *A&A*, 161, 314
- Cunha, K., Smith, V.V., & Lambert, D.L. 1995, *ApJ*, 452, 634
- Davis, S.P., & Phillips, J.G. 1963, *The Red System of the CN Molecule*, University of California Press, Berkeley.
- de Laverny, P., & Gustafsson, B. 1998, *A&A*, 332, 661
- Garz, T. 1973, *A&A*, 26, 471
- Giridhar, S., Lambert, D.L., & Gonzalez, G. 1999, *PASP*, 111, 1269
- Giridhar, S., Lambert, D.L., & Gonzalez, G. 2000, *PASP*, 112, 1559

- Grevesse, N., & Sauval, A.J. 1998, *Space. Sci. Rev.* 85, 161
- Griffin, R. 1974, *MNRAS*, 167, 645
- Gustafsson, B., Karlsson, T., Olsson, E., Edvardsson, B., & Ryde, N. 1999, *A&A*, 342, 426
- Hannaford, P., Lowe, R.M., Grevesse, N., Biéumont, E., & Whaling, W. 1982, *ApJ*, 261, 736
- Hinkle, K., Wallace, L., Valenti, J., & Harmer, D. 2000, *Visible and Near Infrared Atlas of the Arcturus Spectrum 3727 - 9300 Å*
- Hrivnak, B.J. 1995, *ApJ*, 438, 341
- Hrivnak, B.J. 1997, in *IAU Symp. 180, Planetary Nebulae*, ed. H.J. Habing and H.J.G.L.M. Lamers, Dordrecht: Kluwer, 303
- Hrivnak, B.J., & Kwok, S. 1991, *ApJ*, 371, 631
- Hrivnak, B.J., & Kwok, S. 1999, *ApJ*, 513, 869
- Hrivnak, B.J., Kwok, S., & Geballe, T.R. 1994, *ApJ*, 420, 783
- Iben, I.Jr. 1964, *ApJ*, 140, 1631
- Kipper, T., Jorgensen, U.G., Klochkova, V.G., & Panchuk, V.E. 1996, *A&A*, 306, 489
- Kurucz, R.L. 2000, <http://cfaku5.harvard.edu>
- Kurucz, R.L. 1995, <http://cfaku5.harvard.edu>
- Kwok, S. 1993, *ARA&A*, 31, 63
- Kwok, S., Volk, K.M., & Hrivnak, B.J. 1989, *ApJ*, 345, L51
- Lambert, D.L., 1993, in *Molecules in the Stellar Environment*, ed. U.G. Jorgensen, Springer-Verlag (Berlin), 1
- Lambert, D.L., Gustafsson, B., Eriksson, K., & Hinkle, K.H. 1986, *ApJS*, 62, 373
- Lambert, D.L., Heath, J.E., Lemke, M., & Drake, J. 1996, *ApJS*, 103, 183
- Lambert, D.L., Smith, V.V., & Heath, J. 1993, *PASP*, 185, 568
- Lambert, D.L., & Warner, B., 1968, *MNRAS*, 138, 181
- Loup, C., Forveille, T., Omont, A., & Paul, J.F. 1993, *A&AS*, 99, 291

- Luck, R.E., & Bond, H.E. 1991, ApJS, 77, 515
- Meylan, T., Furenlid, I., Wiggs, M.S., & Kurucz, R.L. 1993, ApJS, 85, 163
- Ohnaka, K., Tsuji, T., & Aoki, W. 2000, A&A, 353, 528
- Plez, B., Smith, V.V., & Lambert, D.L. 1993, ApJ, 418, 812
- Prochaska, J.X., & McWilliam, A. 2000, ApJ, 537L, 57
- Reddy, B.E., Bakker, E.J., & Hrivnak, B.J. 1999, ApJ, 524, 831
- Reddy, B.E, Parthasarathy, M., Gonzalez, G., & Bakker, E.J. 1997, A&A, 328,331
- Sackmann, I-J., & Boothroyd, A.I. 1992, ApJ, 392, L71
- Shetrone, M.D., & Sneden, C., & Pilachowski, C.A. 1993, PASP, 105, 337
- Siess, L., & Livio, M. 1999, MNRAS, 304, 925
- Smith, V.V., & Lambert, D.L. 1989, ApJ, 345, L75
- Smith, V.V., & Lambert, D.L. 1990, ApJ, 361, L69
- Smith, G., & Raggett, D.St.J. 1981, J.Phys.B 14, 4015
- Smith, V.V., Shetrone, M.D., & Keane, M.J. 1999, ApJ, 516, 73
- Sneden, C. 1973, Ph.D. thesis, Univ. of Texas at Austin
- Tull, R.G., MacQueen, P.J., Sneden, C., & Lambert, D.L. 1995, PASP, 107, 251
- Van Winckel, H & Reyniers, M. 2000, A&A, 354, 135
- Waelkens, C., Van Winckel, H., Bogaert, E., & Trams, N.R. 1992, A&A, 264, 159
- Whaling, W., Hannaford, P., Lowe, R.M., Biémont, E., & Grevesse, N. 1985, A&A, 153, 109
- Wallace, L., Hinkle, K., & Livingston, W. 1993, An Atlas of the Spectrum of the Solar Photosphere
- Wiese, W.L., Fuhr, J.R., & Deters, T.M. 1996, Atomic Transition Probabilities of Carbon, Nitrogen, and Oxygen: A Critical Data Compilation, American Chemical Society .. for NIST, 453
- Wyller, A.A. 1966, ApJ, 143, 828

Začs, L., Klochkova, V.G., & Panchuk, V.E. 1995, MNRAS, 275,764

Fig. 1.— The spectra of the two pAGBs from 6770 to 6800Å showing s-process lines.

Fig. 2.— The spectra of the two pAGBs from 7955 to 7980Å showing photospheric molecular CN lines (solid vertical marks) in IRAS 05113+1347. Note the absence of these CN lines in the spectrum of IRAS 22272+5435. Telluric spectrum (dotted line) is also shown to indicate the presence of atmospheric lines

Fig. 3.— Determination of atmospheric parameters:  $T_{\text{eff}}$ ,  $\log g$ ,  $\xi_t$ , and  $[M/H]$  using standard excitation and ionization balance among Fe I and Fe II lines. In the top panel, the lower excitation potential (LEP)-abundance relation is used to determine  $T_{\text{eff}}$ . In the middle panel, the reduced equivalent width ( $W_\lambda/\lambda$ )-abundance relation is used to determine  $\xi_t$ , and, in the bottom panel, the abundances of Fe I (crosses) versus Fe II (hexagons) are used in determining  $\log g$ . In all the panels, solid line is the least-squares fit to the data points.

Fig. 4.— Spectra of the two pAGBs showing the circumstellar molecular  $C_2$  (marked by vertical dashed lines) which are strikingly narrow compared to their counterparts in the photospheric spectrum.

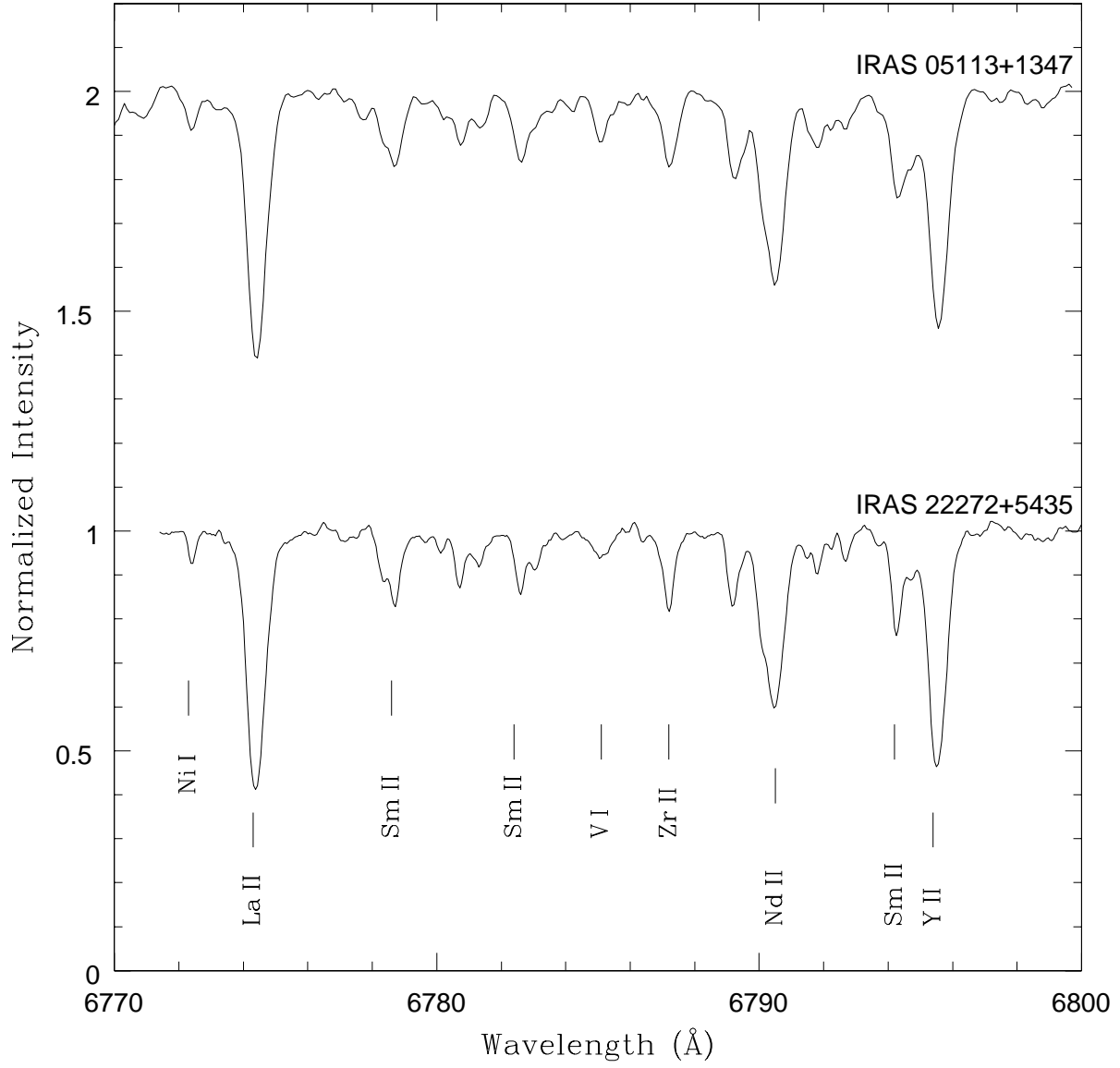
Fig. 5.— Profiles of Li I, Na  $D_1$ , and K I resonance lines (December 31, 1999 spectra) for IRAS 05113+1347. Note the strong emission in the Na I profile which is very well aligned with the central peaks of both the Li (dotted line) and K (broken line) profiles. A predicted K I profile (solid line) based on the derived abundances is also shown.

Fig. 6.— Profiles of Li I (dotted line), Na  $D_1$  (solid line), and K I (broken line) resonance lines for IRAS 22272+5435. Interstellar and telluric lines are marked by  $IS$  and  $\oplus$ , respectively.

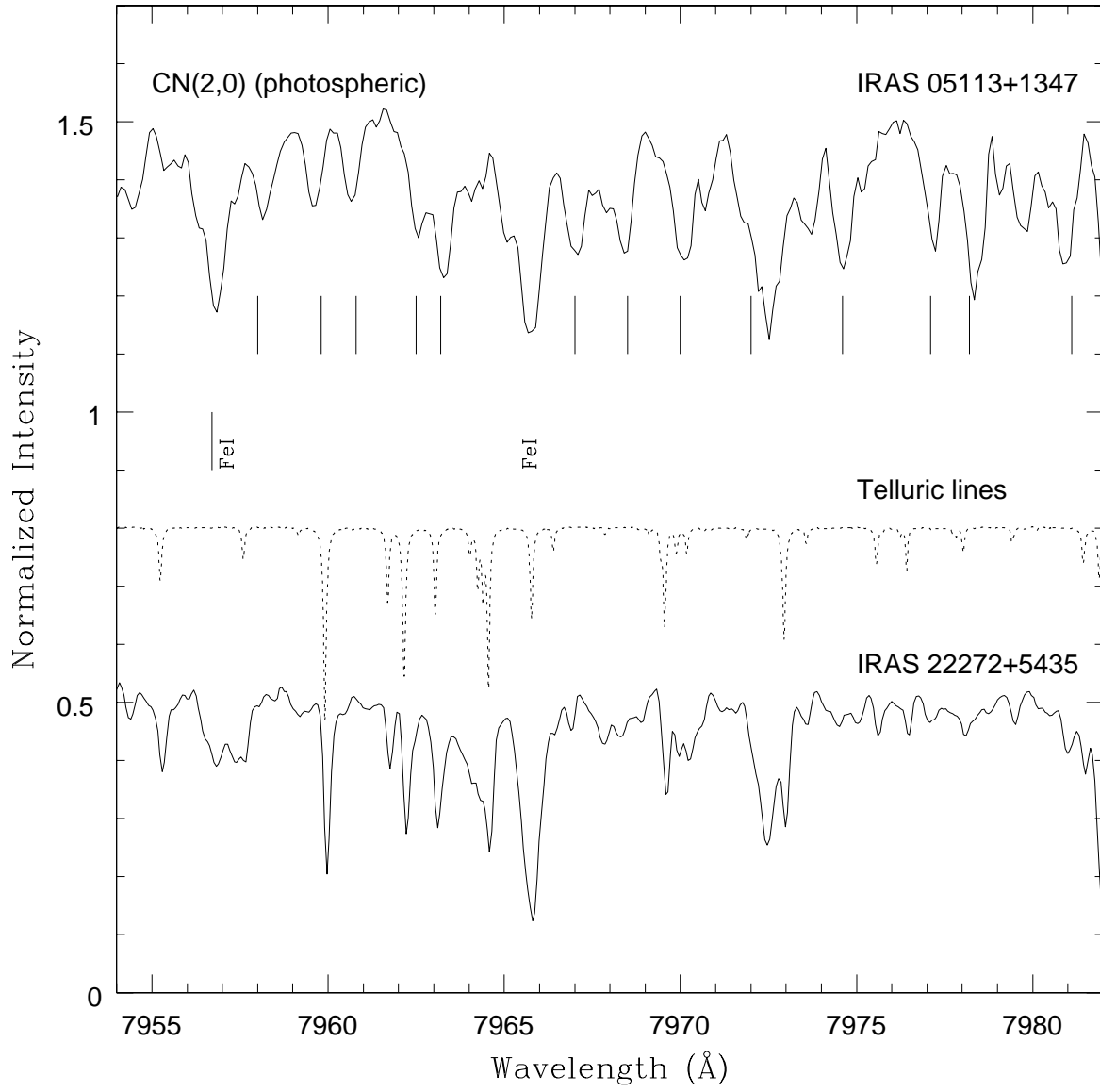
Fig. 7.— Spectrum syntheses of the Li I line at 6707.8Å. Spectrum syntheses (solid lines) with varying Li abundances are compared with the observed Li profiles (dashed lines).

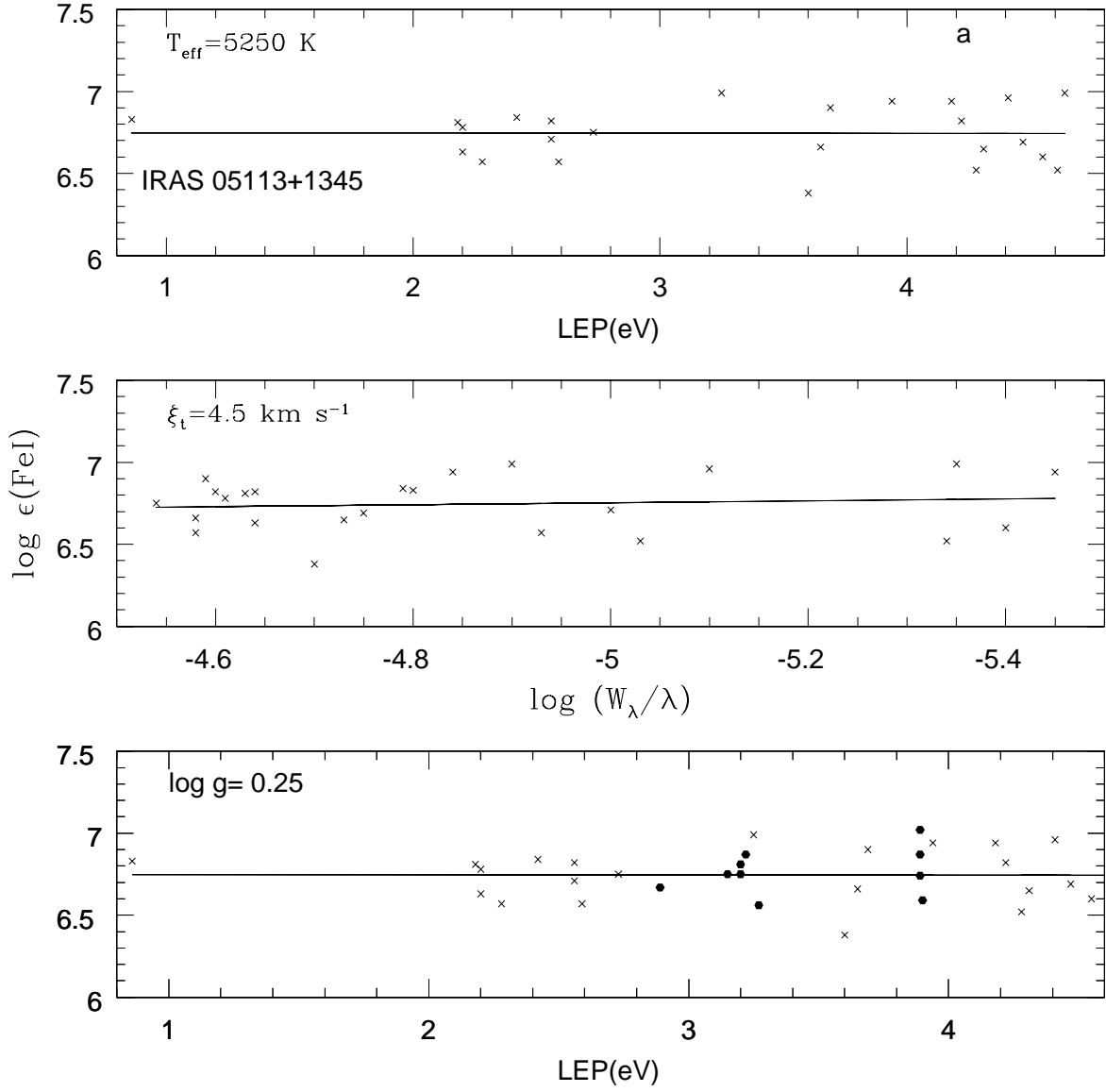
Fig. 8.— Determination of the carbon isotopic ratio  $^{12}C/^{13}C$  for IRAS 05113+1347. The 8001 - 8010Å region was synthesized for three different ratios of  $^{12}C/^{13}C = 25, 15, 5$  (solid lines) and compared with observed spectrum (dashed line). Abundances of C, N, and other elements are kept constant.

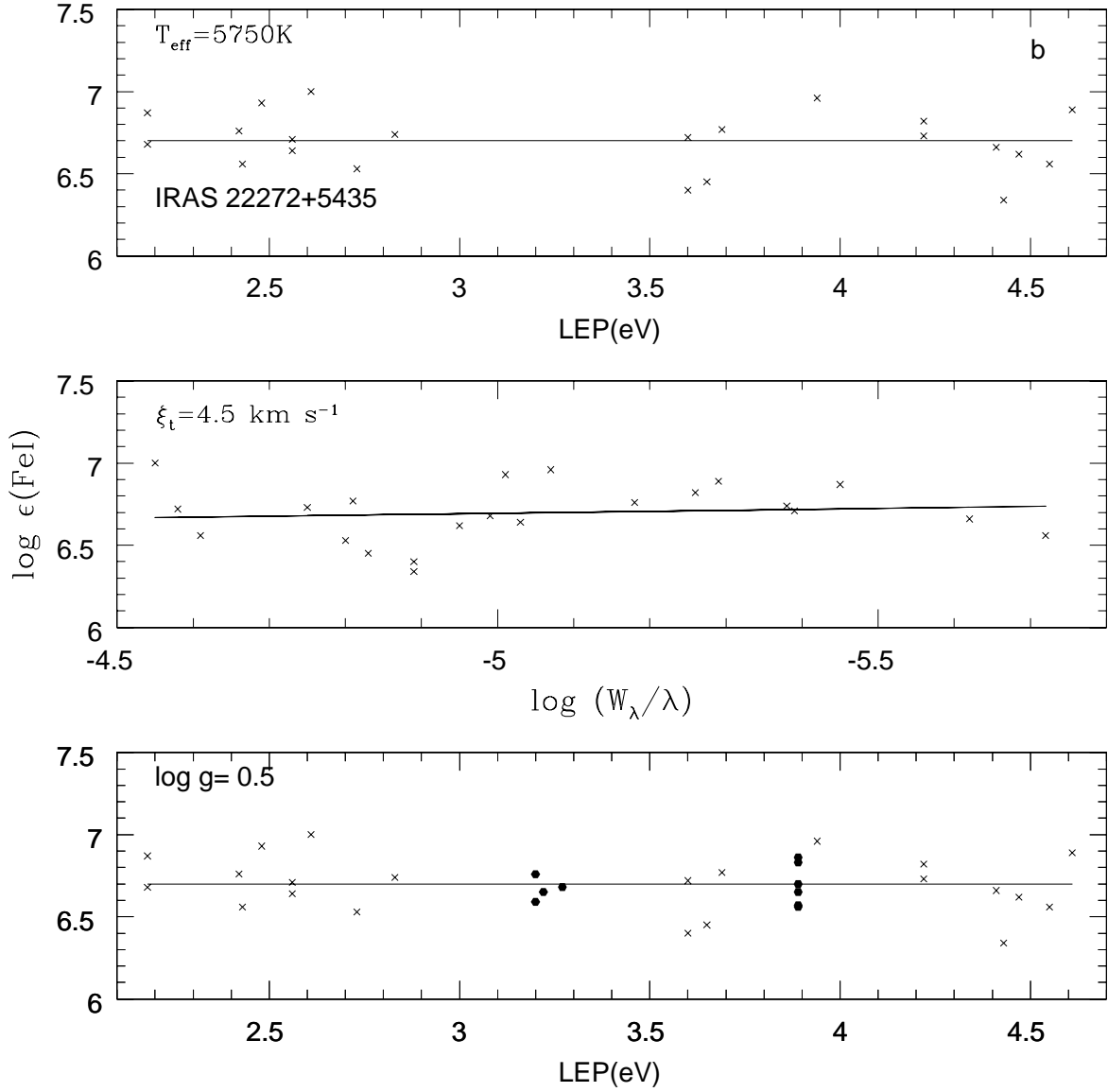
Fig. 9.— Ratios of light (Y,Zr) and heavy (La and Nd) s-process abundance ratios ( $[hs/ls]$ ) of the intrinsic pAGB stars are plotted against metallicity ( $[Fe/H]$ ). Note that  $[hs/ls]$  increases with decreasing metallicity. The dashed line is the predicted  $[hs/ls]$  versus  $[Fe/H]$  curve from Busso et al. (2001) for ST/1.5 of 1.5  $M_\odot$  model

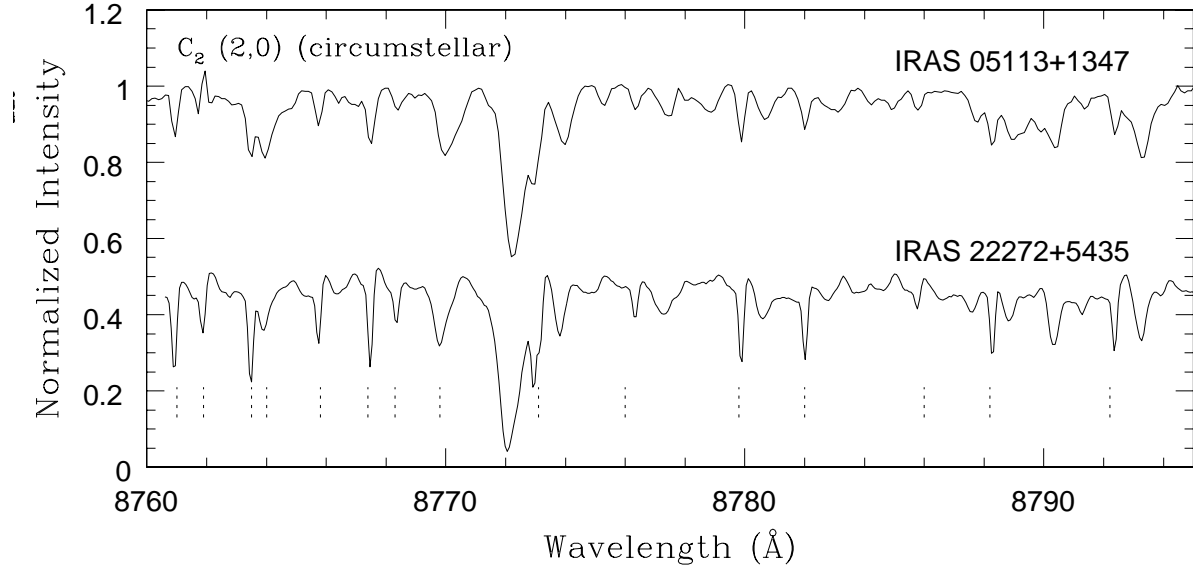


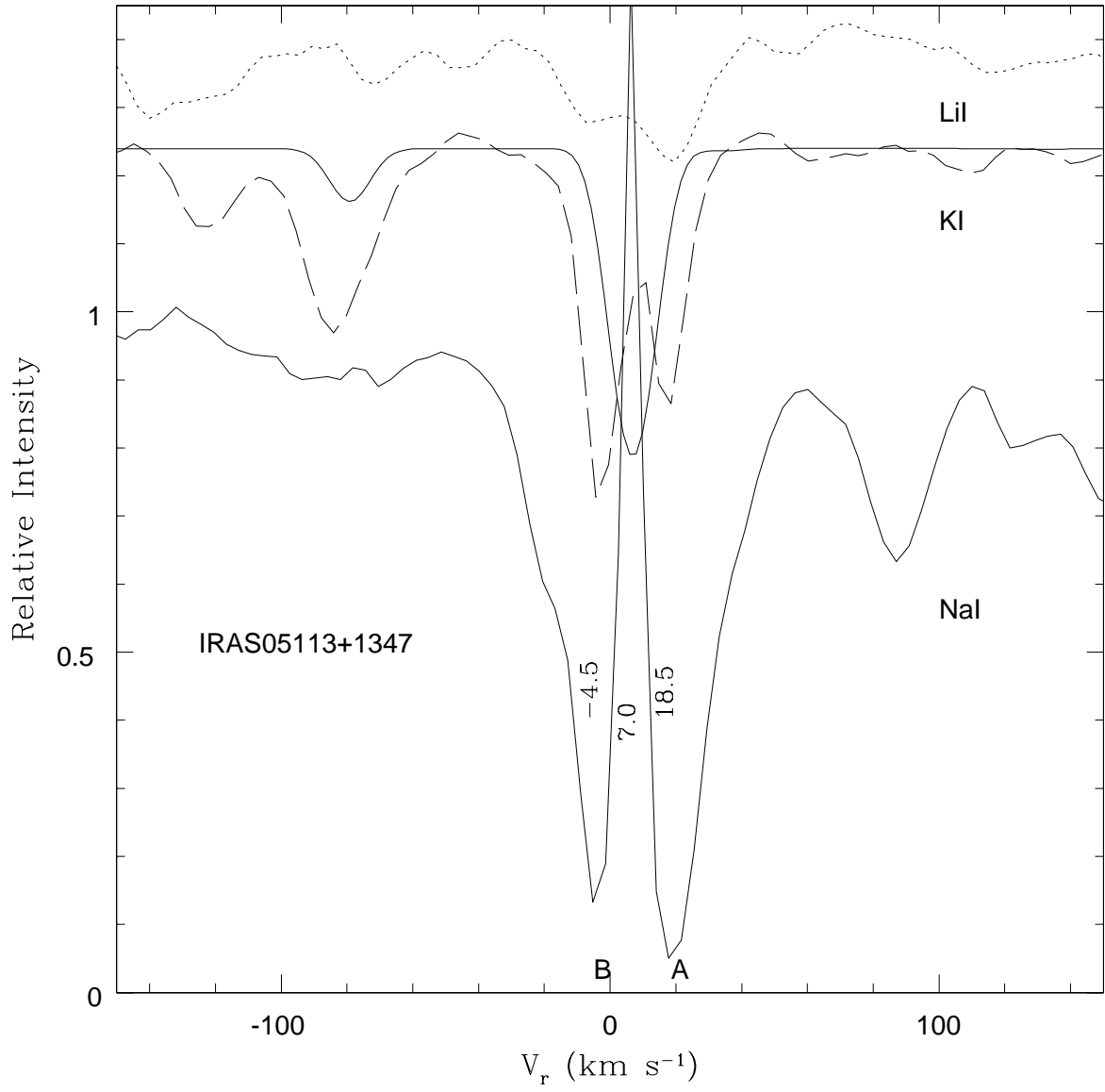


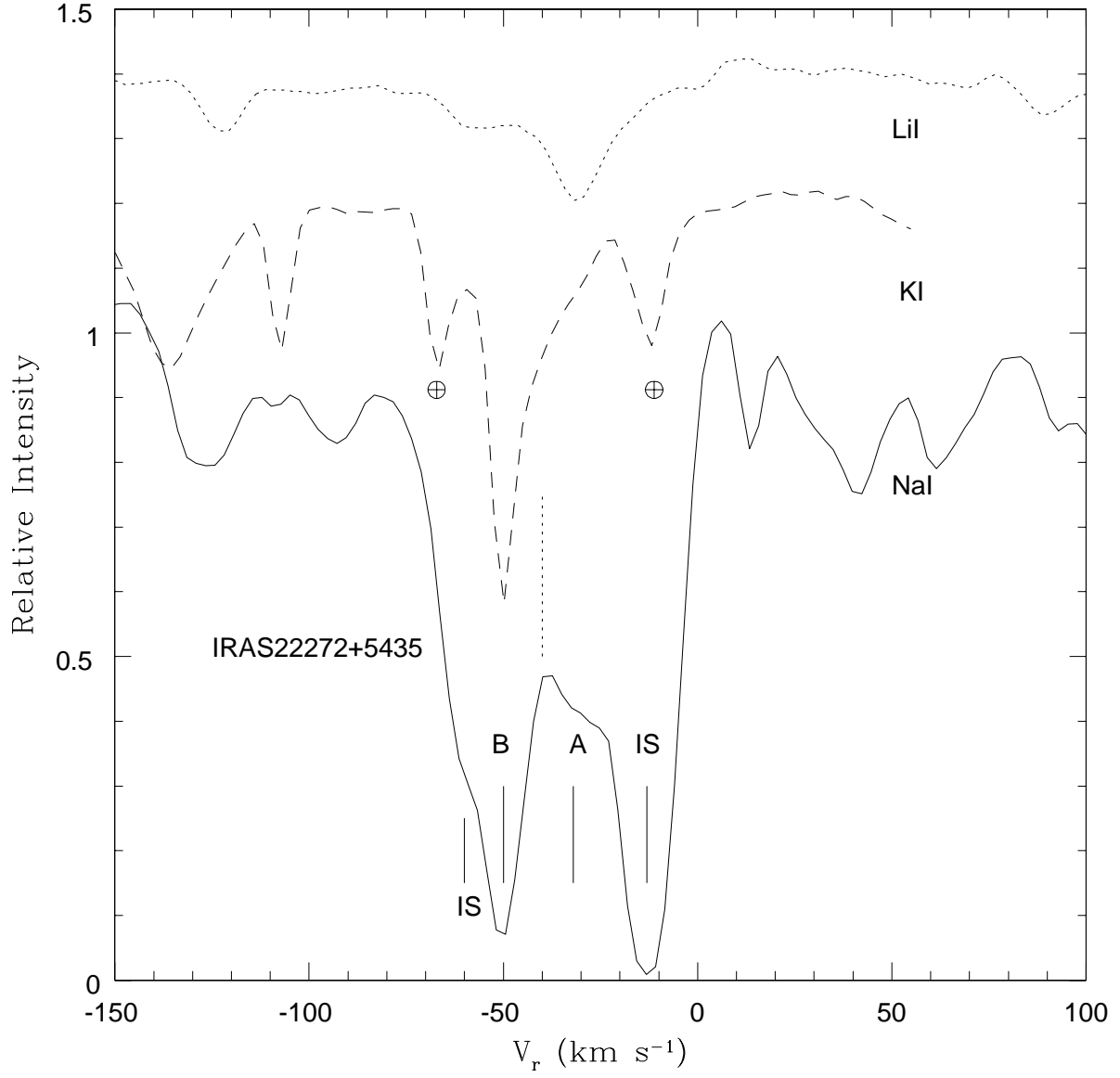


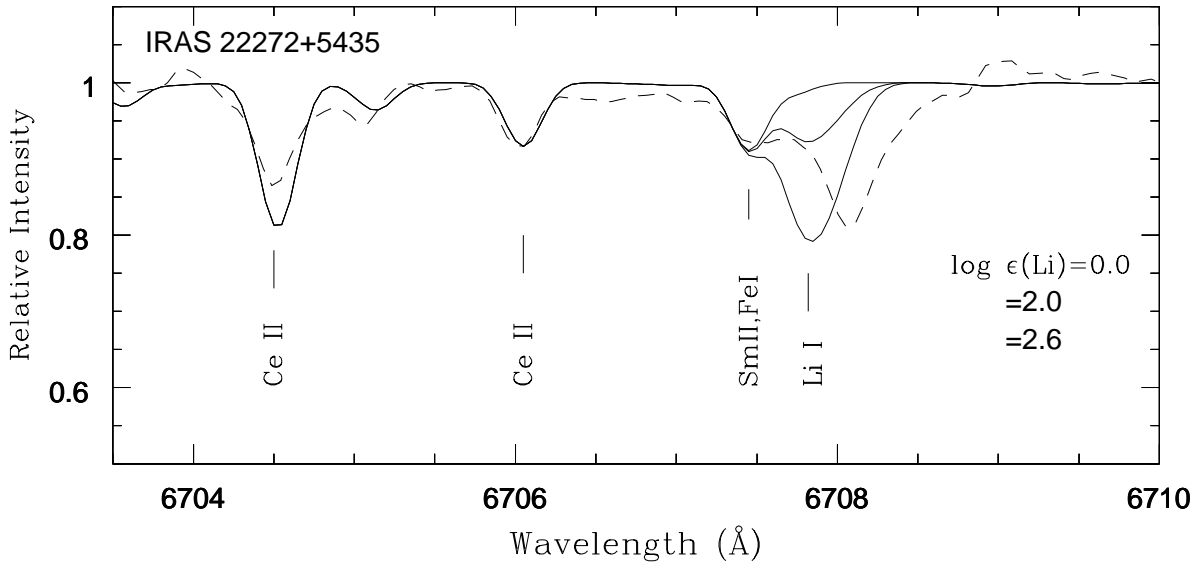
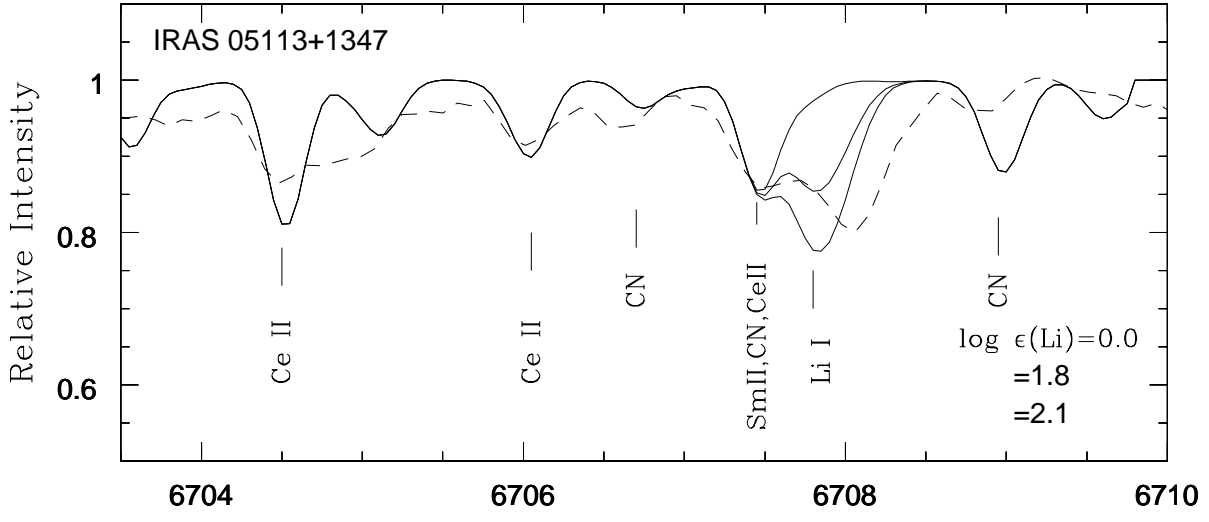


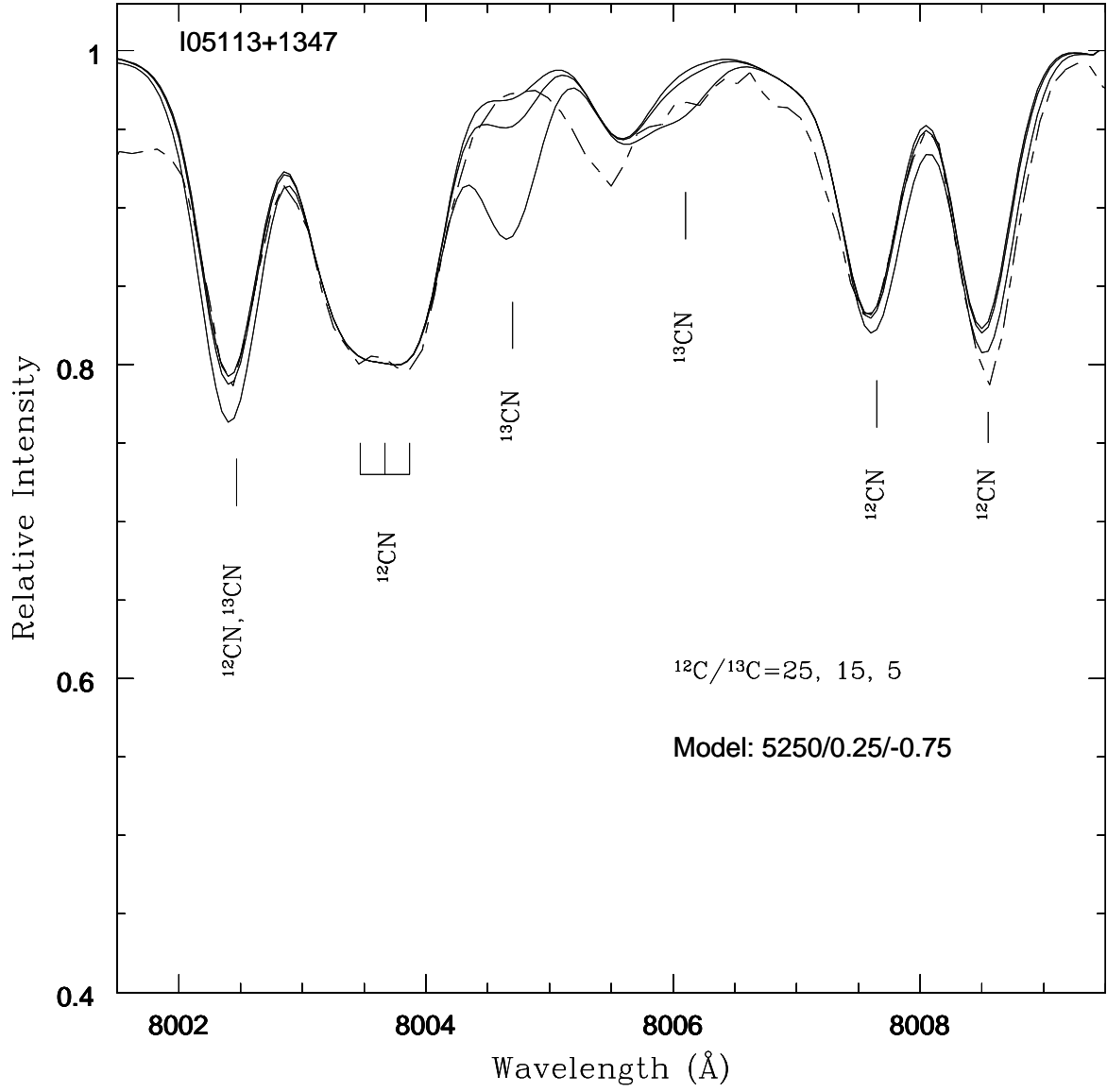














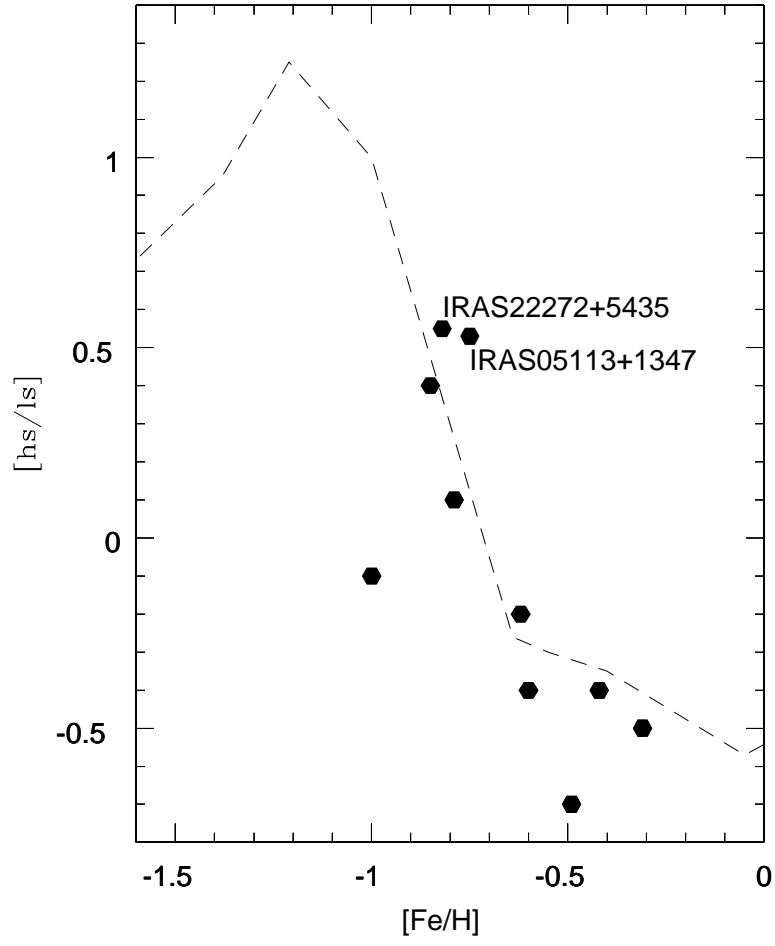


Table 1: Basic Observational Data

	IRAS 05113+1347	IRAS 22272+5435
$m_v$	12.4	8.9
B-V	2.1	1.9
Sp.type	G8Ia	G5Ia
$l$	188.9	103.4
$b$	-14.3	-2.5

Table 2: Derived Spectroscopic Parameters

IRAS	$T_{\text{eff}}$ K	$\log g$ cm s <sup>-2</sup>	$\xi_t$ km s <sup>-1</sup>	[Fe/H]	$V_r$ km s <sup>-1</sup>	$V_{\text{exp}}$ km s <sup>-1</sup>
05113+1347	5250	0.25	4.5	-0.75	7.8	10.1
22272+5435	5750	0.50	4.5	-0.82	-42.3	6.2

Table 3: Heliocentric radial velocity measurements for different species. The expansion velocities ( $V_{exp}$ ) are derived using molecular C2 and CN lines which are originated in the dust envelope

Species	LEP <sup>a</sup>	IRAS 05113+1347			IRAS 22272+5435		
		$n$	$V_r^b$	$\sigma$	$n$	$V_r$	$\sigma$
C I	8.8	4	5.0	1.0	8	−43.4	1.9
N I	10.3	2	10.3	...	2	−43.3	...
S I	8.0	3	8.6	2.5	2	−41.1	...
Si I	5.8	12	6.4	1.1	2	−43.1	...
Fe I	3.5	20	6.5	1.4	17	−42.8	1.2
Fe II	3.6	11	7.8	1.1	33	−41.6	1.5
Ca I	2.5	6	6.8	1.2	6	−42.6	0.8
Sc II	1.4	3	7.1	2.5	3	−42.9	0.6
Pr II	1.2	10	8.6	1.8	6	−42.0	1.5
Sm II	1.4	12	8.4	2.0	5	−41.0	1.0

<sup>a</sup>Average excitation potential (in eV) of the lower state of the transition

<sup>b</sup>Mean radial velocity

Table 4: Abundance Results for pAGB stars: IRAs 05113+1347 and IRAS 22272+5435. Abundances relative to both the solar ( $[X/H]$ ) and the iron ( $[X/Fe]$ ) are given. The  $\sigma$  denotes the scatter among the individual lines and  $n$  represents number of lines used in the analysis.

IRAS 05113+1347						IRAS 22272+5435				
Species	$n$	$\log \epsilon (X)$	$[X/H]$	$[X/Fe]$	$\sigma$	$n$	$\log \epsilon (X)$	$[X/H]$	$[X/Fe]$	$\sigma$
Li	1	1.5 - 2.10	-	-	-	1	2.0 - 2.5	-	-	-
C I	4	8.87	0.35	1.09	0.14	8	8.71	0.17	0.98	0.14
[C I]	1	8.64	0.12	0.87	-	-	-	-	-	-
N I	2	8.23	0.32	1.05	0.11	2	7.68	-0.24	0.57	0.13
O I	1	8.54	-0.29	0.45	-	-	-	-	-	-
[O I]	2	8.37	-0.46	0.29	-	1	8.53	-0.30	0.50	-
Na I	1	5.82	-0.51	0.24	-	2	5.89	-0.44	0.30	0.04
Al I	3	< 5.72	< -0.75	< 0.0	-	2	5.78	-0.69	0.13	...
Si I	4	7.09	-0.46	0.28	0.06	2	7.17	-0.60	0.15	0.06
S I	5	6.87	-0.52	0.23	0.22	6	6.89	-0.60	0.15	0.20
Ca I	6	5.64	-0.72	0.02	0.15	5	5.68	-0.68	0.05	0.18
Ti I	5	4.60	-0.42	0.32	0.09	2	4.55	-0.45	0.37	-
Ti II	5	4.36	-0.66	0.08	0.25	3	4.46	-0.54	0.28	0.11
Cr I	5	4.89	-0.78	-0.04	0.09	5	5.13	-0.54	0.27	0.04
Mn I	3	4.68	-0.78	0.04	0.05	2	4.80	-0.59	0.22	0.15
Fe I	24	6.74	-0.76	0.00	0.17	22	6.70	-0.80	0.00	0.18
Fe II	11	6.77	-0.73	0.00	0.14	13	6.67	-0.83	0.00	0.10
Ni II	12	5.45	-0.80	-0.06	0.16	6	5.53	-0.72	0.02	0.17
Zn I	1	3.74	-0.85	-0.10	-	1	4.16	-0.58	0.23	-
Y II	4	3.36	1.12	1.86	0.07	3	3.28	1.04	1.81	0.14
Zr II	2	3.23	0.63	1.37	0.00	2	3.17	0.57	1.31	0.04
La II	10	2.71	1.49	2.23	0.19	9	2.75	1.53	2.27	0.18
Ce II	12	2.84	1.30	2.04	0.20	6	2.76	1.22	2.03	0.14
Pr II	10	1.63	0.92	2.56	0.20	6	1.61	0.90	1.71	0.21
Nd II	8	2.61	1.11	1.85	0.05	7	2.76	1.30	2.11	0.10
Sm II	12	2.36	1.36	2.10	0.10	5	2.37	1.90	2.71	0.17

Table 5: Uncertainties in the Abundance ratios  $[X/Fe]$  for the C-rich pAGB star IRAS 05113 1347, due to Uncertainties in the Model Atmospheric Parameters

$[X/Fe]$	LEP <sup>a</sup>	$\delta T_{\text{eff}}$	$\delta \log g$	$\delta \xi_t$	$\delta [M/H]$	$\sigma_m$
	Ev	+150 K	+0.50	+0.5 km s <sup>-1</sup>	+0.25 dex	
Fe	3.3	-0.09	-0.06	0.06	0.010	0.12
Cl	8.6	0.24	-0.13	-0.03	-0.01	0.27
[Cl]	1.3	0.05	-0.12	-0.03	-0.03	0.14
N	10.3	0.30	-0.15	-0.04	0.02	0.34
O	0.0	0.09	-0.12	-0.03	-0.02	0.15
Na	2.1	-0.02	0.09	-0.06	-0.01	0.11
Al	4.0	0.03	0.08	-0.02	0.01	0.09
Si	5.8	0.02	0.09	-0.04	0.00	0.10
S	8.1	0.18	-0.10	-0.04	-0.01	0.21
Ca	2.6	-0.05	0.10	0.00	0.01	0.11
Sc	1.4	0.02	-0.12	0.05	-0.02	0.13
Ti I	1.4	-0.11	0.10	-0.04	0.01	0.15
Ti II	2.0	0.05	-0.11	-0.02	-0.02	0.12
V	0.8	-0.12	0.11	-0.06	0.00	0.17
Cr	1.8	-0.09	0.11	-0.02	0.00	0.14
Mn	1.7	-0.12	0.11	-0.04	0.00	0.17
Ni	3.3	-0.08	0.10	-0.02	0.01	0.13
Zn	3.7	-0.06	0.09	0.02	0.01	0.11
Y	1.7	0.02	-0.11	0.03	-0.02	0.12
Zr	2.5	0.05	-0.11	-0.03	-0.03	0.13
La	1.5	0.02	-0.11	0.02	-0.02	0.11
Ce	1.7	0.02	-0.11	-0.03	-0.04	0.12
Pr	1.2	-0.03	-0.09	-0.01	-0.03	0.10
Nd	1.3	-0.03	-0.10	-0.02	-0.03	0.11
Sm	1.3	-0.02	-0.10	-0.04	-0.03	0.11
Eu	1.3	0.00	-0.14	0.03	-0.02	0.15

<sup>a</sup>Average excitation potential (in eV) of the lower state of the transition

Table 6: Abundances of C, N, and O. Ratios are calculated after correcting for initial C and O Abundances at the observed  $[\text{Fe}/\text{H}]$  values.

Star	$[\text{Fe}/\text{H}]$	$\log \epsilon(\text{C})$		$\log \epsilon(\text{N})$		$\log \epsilon(\text{O})$		C/O	N/O	$\Sigma\text{CNO}/\text{Fe}$
		$C_{ini}$	$C_{obs}$	$N_{ini}$	$N_{obs}$	$O_{ini}$	$O_{obs}$			
IRAS 05113+1347	-0.74	7.97	8.81	7.18	8.24	8.31	8.43	2.57	1.07	0.59
IRAS 22272+5435	-0.82	7.90	8.69	7.10	7.68	8.26	8.48	1.82	0.28	0.51
IRAS 02229+6208	-0.45	8.21	8.84	7.47	8.67	8.50	...	...	...	...
IRAS 04296+3429	-0.70	8.00	8.71	7.30	7.76	8.34	...	...	...	...
IRAS 05341+0852	-0.85	7.88	8.73	7.07	7.83	8.24	8.57	1.62	0.33	0.60
IRAS 07134+1005	-1.00	7.76	8.65	7.46	7.84	8.20	8.67	1.15	0.31	0.71
IRAS 07430+1115	-0.46	8.20	8.76	6.92	7.97	8.49	...	...	...	...
IRAS 19500-1709	-0.60	8.09	8.98	7.32	8.37	8.40	8.96	1.05	0.38	0.75
IRAS 22223+4327	-0.46	8.20	8.58	7.61	7.84	8.49	8.50	1.15	0.29	0.20
IRAS 23304+6147	-0.79	7.93	8.70	7.13	7.68	8.28	8.24	3.16	0.48	0.43
Mean Value	-0.69	8.01	8.75	7.26	7.99	8.35	8.55	1.79	0.45	0.54
Sun	0.0	...	8.52	...	7.92	...	8.83	0.49	0.12	0.0

Table 7: Results of Li, CNO, and carbon isotopic ratios for the two pAGB stars are compared with the previously analyzed eight C-rich pAGB stars. Upper limits to lithium abundances are based on assumed detectability limit of 5 mÅ for Li line at 6707Å (See the text for the details).

pAGB	[Fe/H]	log $\epsilon$ (Li)	log $\epsilon$ (N)	$\Sigma CN_{initial}$	$^{12}\text{C}/^{13}\text{C}$	[hs/l <sub>s</sub> ]
IRAS 05113+1347 <sup>1</sup>	-0.74	2.10	8.24	7.9	$\geq 25^1$ $\geq 20^4$	0.4
IRAS 22272+5435 <sup>1</sup>	-0.82	2.60	7.68	7.8	...	0.6
IRAS 02229+6208 <sup>2</sup>	-0.45	2.30	8.67	8.2	$\geq 25^1$	-0.9
IRAS 04296+3429 <sup>3</sup>	-0.70	<2.3	7.84	7.9	$\geq 20^4$	-0.3
IRAS 05341+0852 <sup>2</sup>	-0.85	$\sim 2.5$	7.83	7.8	...	0.6
IRAS 07134+1005 <sup>3</sup>	-1.00	<2.7	7.84	7.6	...	-0.1
IRAS 07430+1115 <sup>2</sup>	-0.46	2.40	7.97	8.2	...	-0.4
IRAS 19500-1709 <sup>3</sup>	-0.60	<3.6	8.37	8.2	...	-0.5
IRAS 22223+4327 <sup>3</sup>	-0.46	<1.9	7.88	8.2	$\geq 20^4$	-0.4
IRAS 23304+6147 <sup>3</sup>	-0.79	<2.1	7.68	7.8	$\geq 20^4$	0.2

References. — (1) This work; (2) Reddy et al. (1996, 1999); (3) van Winckel & Reyniers (2000); (4) Bakker et al. (1996)

Table 8: Atomic Data and Abundances of Individual lines of *s*-process Elements

$\lambda$ (Å)	LEP (eV)	$\log gf$	IRAS 05113+1347		IRAS 22272+5435	
			$W_\lambda$ (mÅ)	$\log \epsilon(X)$	$W_\lambda$ (Å)	$\log \epsilon(X)$
<u>Y II</u>						
6832.47	1.74	-1.940	188	3.36	120	3.12
6951.68	1.84	-2.040	164	3.36	...	...
7332.96	1.72	-2.480	113	3.27	88	3.36
6858.29	1.74	-1.970	196	3.44	150	3.36
<u>Zr II</u>						
6578.65	2.43	-1.500	68.0	3.22	40	3.14
6787.16	2.49	-1.170	102.0	3.23	72	3.19
<u>La II</u>						
6067.12	0.77	-2.340	130	2.58	92	2.66
6126.07	1.25	-1.240	215	2.68	157	2.54
6146.52	0.24	-2.470	180	2.46	143	2.61
6296.08	1.25	-0.950	261	2.76	...	...
6399.03	2.64	-0.530	117	2.71	85	2.67
6446.64	2.76	-0.720	81	2.74	75	2.89
6570.94	0.77	-2.520	142	2.79	118	3.00
6642.76	2.53	-0.960	122	3.04	65	2.79
6714.11	2.76	-0.930	78	2.91	65	2.99
6834.10	0.24	-2.180	219	2.39	185	2.57
<u>Ce II</u>						
7105.05	0.54	-2.526	110.0	3.04	...	...
7486.56	2.55	-0.394	52.0	2.63	...	...
7689.18	1.58	-1.165	115.0	2.84	88	2.98
7313.45	1.93	-0.919	123.0	3.07	54	2.81
6706.05	1.84	-1.253	26.0	2.40	24	2.66
6652.74	1.53	-1.213	152.0	3.17	...	...
6393.03	1.46	-1.242	96.0	2.73	64	2.80
6466.89	1.77	-1.022	104.0	2.91	50	2.75
6973.50	2.32	-0.518	55.0	2.56	33	2.55
7058.69	0.29	-2.761	129.0	3.13	...	...
7061.75	1.93	-0.640	148.0	2.99	...	...
7086.35	2.13	-0.441	98.0	2.65	...	...
<u>Pr II</u>						
6656.83	1.82	0.082	131.0	1.74	66	1.58
6566.76	0.22	-1.721	133.0	1.76	...	...
6429.63	1.61	-0.326	68.0	1.45	...	...



Table 8-Continued

$\lambda$ (Å)	LEP (eV)	$\log gf$	IRAS 05113+1347		IRAS 22272+5435	
			$W_\lambda$ (mÅ)	$\log \epsilon(X)$	$W_\lambda$ (Å)	$\log \epsilon(X)$
<u>Pr II</u>						
6363.63	1.12	-1.419	35.0	1.64	28	1.92
6413.68	1.13	-0.853	...	...	36	1.49
6281.28	0.96	-0.570	117.0	1.36	...	...
6165.89	0.92	-0.205	199.0	1.59	166	1.74
6093.06	1.46	-0.648	39.0	1.32	...	...
6087.53	1.12	-0.618	124.0	1.66	...	...
6086.18	1.30	-0.801	92.0	1.81	...	...
6016.51	1.00	-0.798	152.0	1.92	...	...
6182.34	1.44	-0.387	...	...	33.0	1.31
6046.65	1.12	-0.686	...	...	58.0	1.60
<u>Nd II</u>						
6248.27	1.22	-1.600	93.0	2.56	60	2.67
6250.44	1.16	-1.620	112.0	2.66	79	2.80
6591.43	0.20	-2.510	126.0	2.54	76	2.66
6637.19	1.45	-1.080	143.0	2.63	125	2.88
6650.52	1.95	-0.170	184.0	2.60	147	2.64
6669.63	1.04	-1.720	115.0	2.61	83	2.78
6680.14	1.69	-0.810	148.0	2.66	...	...
6698.64	1.64	-1.360	80.0	2.65	63	2.86
<u>Sm II</u>						
7085.49	1.07	-1.963	100.0	2.52	...	...
6844.70	1.36	-1.529	95.0	2.38	...	...
6734.05	1.37	-1.400	106.0	2.37	83	2.53
6731.81	1.17	-1.372	145.0	2.38	117	2.55
6694.72	1.37	-2.209	30.0	2.43	...	...
6693.56	1.69	-1.089	104.0	2.39	...	...
6679.22	1.07	-1.691	108.0	2.34	...	...
6632.27	1.67	-1.344	53.0	2.19	38	2.33
6616.61	1.35	-2.220	30.0	2.42	...	...
6544.61	1.17	-2.180	30.0	2.18	13	2.14
6542.76	1.17	-1.737	77.0	2.26	45	2.31
6484.55	1.26	-1.792	81.0	2.46	...	...